COST Action FP1402 “Basis of Structural Design” - from research to standards

Short Term Scientific Mission Report

Title: **“Splitting capacity of hardwood connections loaded at an angle to the grain”**

by Dr. **Almudena Majano-Majano**

Technical University of Madrid, ETS Architecture, Department of Building Structures, Madrid, Spain

This report describes collaborative research conducted between 9th November and 16th December 2016.

Host: Dr. José Morais and Dr. José Xavier

University of Trás-os-Montes e Alto Douro, Vila Real, Portugal

Índice

1. Introduction

Connections are one of the most critical parts in timber structures, being the reason of about 80 % of the failures [51]. In particular, dowel-type connections are a very common design solution.

The knowledge of the load-carrying capacity of these type of connections is thus of primordial importance for a rational application, and depends greatly on the failure process and failure mechanisms. These mechanisms can be different according to the connection layout as well as the loading situation. In particular, when connection transfers forces perpendicular to the grain to timber elements, the failure may results either in a ductile failure by yielding of the dowels and/or embedding of the wood underneath the dowel; or a brittle failure by splitting of the timber member at load levels lower than the bearing capacity defined by the ductile embedding of wood and the bending of dowels. This brittle failure could lead to a catastrophic collapse of the whole structure and therefore is the most critical case for the connection failures.

According to current design codes, the ductile failure can be very well predicted by using the European Yield Model proposed by Johansen (1949) [37] and implemented in most international design standards. This analytical model has an empirical basis and assumes and elastic-perfectly plastic behaviour for both wood and dowel. It considers the embedding strength as a material property. This analytical mode however does not take into account the brittle failure characteristic of wood.

The current international design approaches for the prediction of the brittle splitting failure of connections loaded perpendicular to the grain are much different, and are mainly based on a strength criterion (German DIN 1052:2008 [1]); or on an energetic approach in the framework of Fracture Mechanics (Canadian OS86:2009 [5] and European EN 1995-1-1:2016 [3]). The material parameters used in the strength approaches are based on the tensile strength perpendicular to grain $f_{t,90}$, while the fracture energy perpendicular to grain G_I is used in the energetic approaches. It must be noted that some studies suggest that fracture energy rather than perpendicular to grain tensile strength affects the splitting capacity, and thus favours the application fracture mechanics approaches [35]. The apparent fracture energy factor, $\sqrt{GG_c} = 10{,}84\,N/mm^{1,5}$ $\left(= 14\sqrt{0{,}6}\right)$, assumed in the expression included in the European code has been discussed from its origins [11, 12]. Further studies suggest obtaining an individual factor for each specie or product [16] as no values of G_I are specified in the EN 1995-1-1:2016 or the related product standars. Therefore a comprehensive experimental determination of this parameter for each specie would be desirable.

Current researches show that there are disagreements between experimental and numerical results and the analytical design equations included at the mentioned international design standards for the prediction of the splitting failure of connections (e.g. [13, 30, 34]). The splitting capacity depends on different parameters related, among others, to the connection layout, fastener type, loading case... that were not all considered to derive the main code equation. In addition, most of the studies have been focused on wood or wood products made of softwoods. In fact, it is expressly advised at the EN 1995-1-1:2016 [3] that such splitting capacity equation for dowel-type connections *is only valid for softwoods*.

The use of hardwood species for structural purposes is growing increasingly, as is demonstrated by the development of laminated hardwood products and the ongoing research projects to study structural outdoor applications with hardwoods of high durability. Therefore, it becomes necessary to study the applicability to hardwoods of the mentioned analytical equations included in the EN 1995-1-1:2006 to account the splitting capacity of dowel connections loaded ad an angle to the grain. Furthermore, the dowel-to-edges distances for hardwoods also require a review as their high mechanical performance usually involve smaller sections leading to less space for placing multiple fasteners. Since the wood member size is often determined by the connection size, it is advisable to check the dowel-to-edges distances in hardwoods with the aim to optimize the sections.

2. Objectives of the work

The main objective of the present work is to study the splitting failure behaviour of steel dowel-type connections in hardwood members loaded perpendicular to grain. Experimental and numerical research has been carried out for this purpose. *Eucalyptus globulus* Labill has been chosen as hardwood species for this work because the growing interest due to its high mechanical properties. In addition, Galicia region (Spain) and Portugal (countries of home and host institutions respectively of this STSM) form a coastal strip containing the most productive forests in Europe of eucalyptus plantations.

Experimental test series with single and double dowel-type connections following different loaded edged distances layouts are conducted to derive the splitting failure behavior. The correlation between the experimental failure loads obtained and the theoretically ones predicted by different analytical models included in literature (and also compiled in the present report) are discussed. Also the applicability to eucalyptus of the analytical splitting equation included in the EN 1995-1-1:2006 for softwoods along with the required dowel-to-edges distances are argued.

A numerical 2D FEM fracture mechanics model that allows the simulation of both ductile and brittle failure behaviour of the connections using cohesive elements is developed. The correlation between the experimental and numerical results is presented. The numerical model opens the possibility to conduct further parametric studies taking advantage of the effectiveness with regard to time and certainty of results.

The different analytical models compiled in literature to predict the splitting failure in connections loaded perpendicular to grain and also the numerical model requires, as input material properties, the modulus of elasticiy, the shear modulus, the tension strength perpendicular to the grain and the fracture energy. The latter assumes a combined Mode I and Mode II interactions of fracture energy based on relationship between tension perpendicular to the grain and shear stresses [25]. However, a simplifying assumption of fracture energy based only in Mode I fracture has been hitherto accepted as a reasonably accurate approximation in the different literature models [42]. As none of these values are specified in codes, the experimental determination of the Mode I fracture energy of *Eucalyptus globulus* becomes another objective of the present work. Also Mode II fracture energy is determined in order to get a more accurate numerical modelling of the connections following a mixed mode loading. The respective fracture energies are determined from the Resistance curves (R-curves) following the innovative *Compliance-Based Beam Method* (CBBM). The rest of the mentioned material parameters are taken from previous researches using this species.

3. Background of analytical and numerical models and code design approaches

In most international timber design codes, specified minimum edge distances have traditionally been used as sufficient guarantee against brittle splitting failure in connections loaded perpendicular to the grain. Some design codes require also an additional checking of shear stresses at the connection location. However, it is only recently that explicit equations against splitting failure have been included in most design codes for timber. Those are mainly based on: (i) a *strength criterion* (German DIN 1052:2008); (ii) on an *energetic approach* in the framework of Fracture Mechanics (Canadian OS86:2009; European EN 1995-1-1:2016).

In particular, the formula embodied in the DIN 1052:2008 is based on the work carried out by Ehlbeck *et al.* (1989) [27] from empirical and theoretical considerations, which assumes a non-linear influence of the beam dimensions, the loaded edge distance, the connection geometry and the **tensile strength perpendicular to grain,** $f_{t,90}$.

On the other hand, the prediction formula included in the Eurocode 5 was developed afterwards based on an analytical model presented by Van der Put (2000) [54] following the Linear Elastic Fracture Mechanics (LEFM) approach and calibrated also with the data results of Ehlbeck *et al.* In contrast to the DIN 1052:2008, it assumes a linear effect of the beam thickness, a different influence of the loaded edge distance, no effect of the connection geometry, and the **fracture energy**, G_f, as some of the input parameters. It must be noted that some studies suggest that fracture energy rather than perpendicular to grain tensile strength affects the splitting capacity, and thus favours the application of fracture mechanics approaches which will be the focus of this work.

The mentioned theoretical model of Van der Put and also other simple analytical fracture mechanics models presented in recent years for prediction of the splitting failure in timber connections loaded perpendicular to the grain are compiled in the present section (comprehensive review of those approaches are found e.g. in Schoenmakers (2010) [30] and Jensen *et al.* (2015) [36] in more detail). As will be seen, most of these models are related and appear as special cases of a general one, and are based on the energy balance approach [49] and the compliance method of fracture mechanics according to the Eq. 1:

$$P_u = \sqrt{\frac{2G_f}{\frac{dC(A)}{dA}}} \tag{1}$$

being A and C de crack area and the compliance of the model respectively.

The different analytical models reviewed next are derived by means of the previous Eq. 1 by making certain assumptions about how to calculate the compliance $C(A)$, which leads to a good agreement with the experimental data. The external load is assumed to act in a single point at the middle of the beam.

The parameters accounted for by the models are:

G_f: fracture energy.

G: shear modulus of elasticity.

E: longitudinal modulus of elasticity.

b: beam width.

h: beam height.

h_e: distance from the connector to the load edge of the beam.

$\alpha = h_e/h$: relative connection height.

a: crack length.

β_s: shear correction factor (6/5 for a rectangular cross section according to ordinary beam theory).

One of the most general models has been formulated by Jensen (2005a) [32] considering a beam structure to model the cracked beam. The failure load leads to the form (Eq. 2):

$$P_u = 2b\sqrt{\frac{2GG_f h_e}{3\frac{G}{E}\left(\frac{a}{h_e}\right)^2 (1-\alpha^3) + \beta_s (1-\alpha)}} \tag{2}$$

A special case of the previous formuation is recently proposed by Jensen *et al.* (2015) [36] when asumming $h \to \infty$ for a finite value of h_e (i.e., $\alpha \to 0$), that is, all beams except the beam with depth $h_e$are assumed to be infinitely stiff. It results in the Eq. 3:

$$P_u = 2b\sqrt{\frac{2GG_f h_e}{3\frac{G}{E}\left(\frac{a}{h_e}\right)^2 + \beta_s}} \tag{3}$$

When only shear deformations are considered and so bending deformations are neglected (i.e., a finite G and $E \to \infty$), the relation $G/E = 0$ and the previous Eq. 3 is reduced to Eq. 4:

$$P_u = 2b\sqrt{\frac{2GG_f h_e}{\beta_s}} \tag{4}$$

This last equation is similar to the solution proped by Larsen and Gustafsson (2001) [26] if $\beta_s = 1$ is assumed.

The analytical model proposed by Van der Put and Leijten (2000) [54] is related also to the previous expressions. In fact, it could be considered also a special case of the general model presented in Eq. 2 if finite G and $E \to \infty$is accounted. The model would thus reduce to Eq. 5:

$$P_u = 2b\sqrt{\frac{2GG_f h_e}{\beta_s (1-\alpha)}} \tag{5}$$

for $\beta_s = 6/5$, the Van der Put equation (Eq. 5) could also be written as:

$$P_u = 2bC_1\sqrt{\frac{h_e}{1-\frac{h_e}{h}}} \tag{6}$$

$$C_1 = \sqrt{\frac{5}{3}GG_f} \tag{7}$$

In cases when $\alpha \to 0$, the previous Eq. 5 would lead to the solution presented in Eq. 4.

Other simply model is the proposed by Ballerini (2004) [38] in an effort to achieve a better fitting to experimental data than using the formula presented by van der Put (Eq. 8) for a single-dowel connection:

$$P_u = 2bC_1\sqrt{\frac{h_e}{1-\alpha^3}} \tag{8}$$

For multiple-dowel connections, a more complex approach is also proposed by the same author [38] (Eq. 9) which include the parameters f_w and f_r based on the connection dimensions and row number of fasteners:

$$P_u = 2bC_1\sqrt{\frac{\alpha h}{(1-\alpha^3)}}f_w\,f_r \tag{9}$$

Other models based on the Timoshenko beam on a Winkler foundation has been postulated by Jensen (2005c) [33]. For a single load acting far from the end of a beam and small crack lengths, the failure load is given by Eqs. 10-12:

$$P_u = \gamma P_{u,\mathrm{LEFM}} \tag{10}$$

$$P_{u,\mathrm{LEFM}} = 2bC_1\sqrt{h_e} \tag{11}$$

$$C_1 = \sqrt{\frac{5}{3}GG_f} \tag{12}$$

being $\gamma = \frac{\sqrt{2\zeta+1}}{\zeta+1}$ the effectiveness factor, with $\zeta = \frac{C_1}{f_t}\sqrt{10\frac{G}{E}\frac{1}{h_e}}$.

Eqs. 10 include the tensile strength parameter f_t in the parameter ζ, and the splitting failure load is not proportional to the square root of the fracture energy. Therefore, the solutions can not be enclosed within linear elastic fracture mechanics (LEFM) nor in non-linear fracture mechanics (NLEFM). They belong to the quasi-nonlinear fracture mechanics [22], and the LEFM solutions are considered as special cases from it.

If assuming $E \to \infty$ or $f_t \to \infty$ at the previous analytical approach, the solution $P_u = P_{u,\mathrm{LEFM}}$ would be obtained. This solution could also be got from Eq. 4 for $\beta_s = 6/5$, and from Eq. 6

for $h \to \infty$ (i.e. $\alpha \to 0$). Because of this latter, it seems feasible to substitute the $P_{u,\mathrm{LEFM}}$with the form given by Eq. 6 into Eq. 10, leading to Eqs. 13-14:

$$P_u = \gamma P_{u,\mathrm{LEFM}} \tag{13}$$

$$P_{u,\mathrm{LEFM}} = 2bC_1\sqrt{\frac{h_e}{1-\frac{h_e}{h}}} \tag{14}$$

For $h \to \infty$, Eqs. 13-14 reduce to Eqs. 10-11, and for $f_t \to \infty$ or $E \to \infty$ they reduce to 6.

An extension of Eq. 10 is proposed by Jensen (2005d) [34] considering also the influence of fastener´s distance from the beam end, l_e leading to Eq. 15, wich could be also generalized by introducing the $P_{u,\mathrm{LEFM}}$ value as is done before for Eq. 10.

$$P_u = P_{u,\mathrm{LEFM}} \cdot \text{mín}\left(\begin{array}{c} \frac{1}{2\sqrt{2\zeta+1}} + \frac{b\,f_t l_e}{P_{u,\mathrm{LEFM}}} \\ \frac{\sqrt{2\zeta+1}}{\zeta+1} \end{array} \right) \tag{15}$$

All the previous models are alike acceptable from a modeling point of view. From a practical design, simple and robust models seem to be more attractive.

In particular, the design approach adopted in the EN 1995-1-1:2016 [3] is based, as mentioned before, on the studies of van der Put [53, 54]. It considers the verification of the shear force acting in the beam as shown in Fig. 1, by fulfilling the Eqs. 16-17.

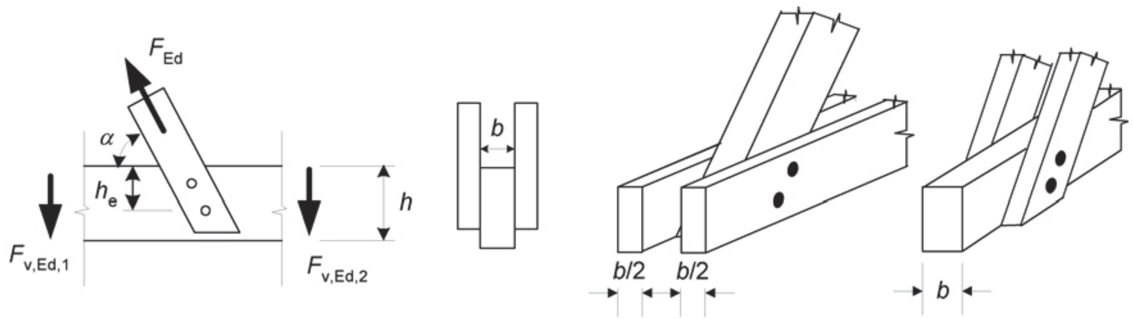

Figura 1: Connections loaded at an angle to the grain according to EN 1995-1-1:2016 [3].

$$F_{v,Ed} \leq F_{90,Rd} \tag{16}$$

being $F_{v,Ed} = max \begin{cases} F_{v,Ed,1} \\ F_{v,Ed,2} \end{cases}$ the design shear forces acting at both sides of the joint.

For softwoods connected by fasteners different from punched metal plates type, the characteristic value of the splitting load is described in the code by the Eq. 17:

$$F_{90,Rk} = bC_1\sqrt{\frac{h_e}{1-\frac{h_e}{h}}} \quad (17)$$

where $C_1 = 14\,\mathrm{N/mm}^{1{,}5}$. This value derives from what is known as *apparent fracture parameter*, $\sqrt{GG_c}$ including in the Eq. 7, representing the square root of the shear modulus times critical energy release rate.

A limitation of the analytical model of the Eurocode 5 is that its fundamental equations were essentially derived for a single row of dowel connections placed at the mid-span of a simply supported beam subjected to a point load (Eqs. 5-6 [53]). Considering the shear forces as described in the Eurocode 5, other different support conditions and connection locations could be handle by the designer.

For a simply supported beam loaded at midspan, Eqs. 5-6 and 16-17 lead to the same failure load if $C_1 = 14\,\mathrm{N/mm}^{1{,}5}$.

Several experimental studies have been addressed to date to enhance those formulae taking into account the effect of some parameters in detail, such as dowel spacing, different connection layouts, different mechanical fasteners, other loading cases, etc [43, 50, 41, 39], but there is still not a general agreement between the results. This empirical way of investigation has been time consuming and not-always cost-efficient.

Another way to achieve these objectives is to simulate the load-carrying capacity of the connections using numerical models by applying the Finite Element Method (FEM). The advantages of numerical simulations are their effectiveness with regard to time, cost, certainty of results and the possibility to conduct parametric studies.

In the recent past, many numerical 2D and 3D FEM models have been developed taking into account elastic or elasto-plastic laws of the material. These models are realistic when a ductile failure is produced. However, they do not reproduce brittle failures [18, 17]. For overcoming this fact, some models have been developed applying the Linear Elastic Fracture Mechanics (LEFM) criteria, where a initial defect or crack must be defined a priori [48, 40]. However its localization in a real structure may not be so obvious in advance.

Recently, the use of cohesive models in the frame of Non Linear Elastic Fracture Mechanics (NLEFM) are of great relevance as the consideration of an initial defect in the material becomes unnecessary and the whole crack growth can be properly simulated being closer to the real behaviour of the structure.

Some of the numerical publications that analyse the splitting capacity of dowel-type connections using cohesive models have chosen 2D formulations by regarding the plane perpendicular to the loading direction [15]. Also a few 3D studies which analysed the splitting behaviour of dowel-type connections using cohesive models have been carried out so far. E.g., Schoenmakers (2010) [30] adopted in his PhD Thesis a cohesive element approach to simulate the crack propagation in beams loaded perpendicular to the grain by multiple connections. Franke and Quenneville (2011) [14] presented an approach based on numerical models and calibrated by tests considering the geometry of the connection, number of rows of fasteners, and the fracture energy parameter in both Mode I (tension perpendicular to grain) and Mode II (shear) failures. Resch and Kaliske (2012) [21] applied it to analyse the influence of some parameters on the load capacity of double-shear single dowel-type connections producing shear and tension failures. Caldeira *et al.* (2014) [55] considered a mixed-mode (I/II/III) cohesive zone modelling in a 3D FEM analysis to determine the quasi-static behaviour of moment-carrying steel-wood doweled joints. A recent numerical investigation using a cohesive model was performed by Santos *et al.* (2015) [19] to study the non-linear behaviour and collapse prediction of T-joints with a single steel dowel and different constitutive modelling approaches for the wood members.

4. Experimental research

Experimental studies on the failure behavior of steel dowel-type connections in hardwood members loaded perpendicular to grain are presented in the present section. It is divided in two parts:

1. Fracture characterization tests in order to get mode I and mode II fracture energies needed to be implemented in numerical and analytical models of the connections for further validation.

2. Single and double dowel type-connection tests to derive the splitting failure behavior following different loaded edged distances configurations. The results are compared to the theoretical values predicted by the different analytical models included in literature and Eurocode 5.

As mentioned before, all the experimental tests have been carried out using *Eucalyptus globulus* Labill as hardwood species. The main interest and characteristics of this material is also presented in the next section.

4.1. Material

Together with beech and ash, *Eucalyptus globulus* is one of the hardwood species growing in Europe with higher mechanical performance (D40, according to EN 1912:2012 [2]). In addition, *Eucalyptus globulus* from Galicia (Spain) also exhibits good natural durability (class 2 against fungi according to prEN 350-2:2014 [6]) comparable to that of chestnut and oak, making it suitable for outdoor applications.

Despite these advantages, the main use of this species is as raw-material for the wood pulp industry. Recent studies have assessed the suitability of *Eucalyptus globulus* for the production of structural and non-structural glued laminated timber, focusing on the processing stages (sawing and drying) as well as on mechanical characterization of the material and gluing properties [52]. These suggest that the main hindrance to marketing is the drying process, which may lead to important material deformations.

Currently several companies together with the University of Santiago de Compostela in Spain are carrying out research projects to develop high performance structural applications using *Eucalyptus globulus* for both indoor and outdoor uses [7, 8] and to improve the drying process [10]. In particular the “LIGNUM” project [8], carried out in collaboration with companies, focused on the development of an Eucalyptus shaft for a new wind turbine (fig. 2 left) among other objectives. Another ongoing research project is the entiteled “EUCAGRID” [9], which aims to deepen the understanding of the mechanical and structural properties of *Eucalyptus globulus* for its innovative implementation in gridshell structures (fig. 2 right).

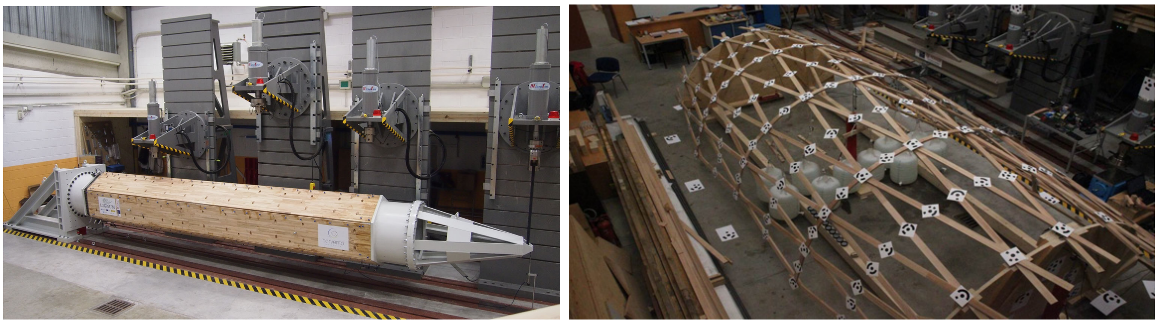

Figura 2: Testing of a wind turbine shaft [8] (left) and of a gridshell structure [9] (right), both made of *Eucalyptus glubulus*.

This confirms the increasing interest in the use of this competitive structural species undergone of development.

Eucalyptus globulus Labill. from the Galicia region (Spain) was used in the present research. Kiln-dried boards cut from heartwood (with no juvenile wood) were prepared. It is worth noting that the boards were approximately free from knots (knot diameter less than 1/20 times the board width). This often occurs in *Eucalyptus globulus* because it develops natural pruning, so from start knots are few and very small.

The boards were conditioned at 20ºC and 65 % relative humidity before sample preparation, until equilibrium moisture content of 12.8 % was reached. Each of the boards is identified with a reference number included in Table 1. This numer will also identify the corresponding specimens obtained from them used in the different series of tests. The densities (ρ) were determined for a reference moisture content of 12 %. The static longitudinal modulus of elasticity in the grain direction (E_L) of these particular boards resulting from an edgewise bending test under four-point loading according to EN 408:2011 [4] was obtained in previous experimental campaigns. These values are considered in the present research and summarized in Table 1.

In addition, the values of the radial modulus of elasticity E_R, shear modulus of elasticity G_{LR} and tensile strength perpendicular to grain $f_{t,90}$ of the material are needed for the fracture characterization research, and the last two also as data for the analytical models. The rest of orthotropic parameters must be used as inputs of the numerical model. These values are

Tabla 1: Material parameters of Eucalyptus boards.

test serie	board reference	ρ $[kg/m^3]$	E_L $[MPa]$
fracture characterization	140	781.1	19863
	144	764.7	19234
	161	866.7	19658
	176	779.0	19359
	189	748.0	19114
	192	814.6	20612
connections	143	787.0	20777
	154	840.0	18592
	168	753.6	19967
	183	776.9	18277
	184	829.1	18502
	187	788.0	19028
	188	847.5	20169

taken from previous experimental campaigns of the author using galician *Eucalyptus globulus* with similar density as the boards referred before. These values are all included in Table 2.

Tabla 2: Orthotropic parameters and tension strength perpendicular to grain of Eucalyptus globulus.

parameters	Value
E_L $[MPa]$	*values in Table 1
E_R $[MPa]$	1820 MPa
E_T $[MPa]$	821
G_{LR} $[MPa]$	1926
G_{LT} $[MPa]$	969
G_{RT} $[MPa]$	533
υ_{RT}	0.635
υ_{LT}	0.606
υ_{LR}	0.448
υ_{TR}	0.325
υ_{RL}	0.032
υ_{TL}	0.032
$f_{t,90}[MPa]$	7.5

4.2. Fracture characterization tests

This section presents the experimental research carried out in order to obtain the fracture parameters of *Eucalyptus globulus* under pure mode I (DCB tests) and mode II (ENF tests) in RL propagation system. The respective critical fracture energies (G_{Ic} and G_{II}) are determined from the Resistance curves (R-curves) following the innovative *Compliance-Based Beam Method* (CBBM), whose basis is explained in the following subsections. These fracture parameters are needed for their implementation in the numerical model of the connections loaded perpendicular to the grain and also for the validation of the existing analytical models in this regard. In addition, the cohesive laws for this material are obtained.

4.2.1. Mode I fracture parameters: Double Cantilever Beam test (DCB) method

The DCB specimen consisted of a rectangular beam with nominal dimensions of 250 mm x 20 mm x 20 mm as is schematically represented in Fig 3. Fifteen specimenes were prepared with axes oriented along the RL propagation system. A mid-height pre-cracked surface with a_0 length of 101 mm is initially made. The crack was generated by using a band saw of 1 mm thickness followed by an impacted blade. With this procedure the effective initial crack length can slightly vary among specimens due to uncertainties in controlling the impact load. Nevertheless, a sharp initial crack surface can be guaranteed and the a_0 value measured accurately for each specimen after testing. A symmetrical pairs of holes of 3 mm diameter are drilled at a distance of 10 mm from the specimen end, where a load (P) perpendicular to the pre-cracked surface is applied. The applied load is transferred to the specimen by means of two steel pins of 3 mm diameter inserted into the drilled holes of the specimens (Fig. 4). Steady-state crack propagation is assumed to occur along the ligament. The tests were carried out in a conventional Instron® testing machine at crosshead displacement rate of 3 mm/min. During the loading process, the applied load (P) and the cross-head displacement (δ) are recorded with a frequency of 5 Hz.

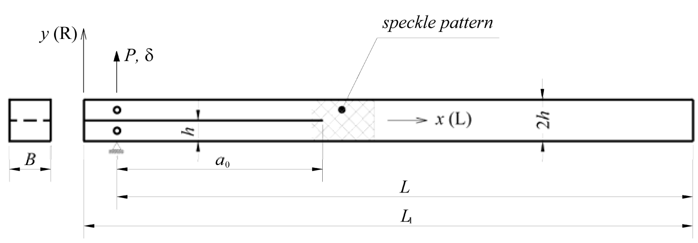

Figura 3: DCB specimen geometry ($2h$ = 20 mm, B = 20 mm, L_1 = 250 mm, L = 240 mm and a_0 = 101 mm).

Fig. 4 shows the DCB test coupled with a digital imagen correlation (DIC) system, ARAMIS 2D. It is used to measure the crack tip opening displacemts (CTOD, w_I) produced in the vicinity of the crack tip needed to obtain the cohesive law of the material. For a complex material such as wood, this technique can be very advantageous in comparison with other standard monitoring procedures. A speckled pattern is painted over the region of interest by means of and airbrush. A textured pattern with suitable granulometry at the scale of magnification, contrast and isotropy was obtained with this marking technique (Fig. 5). An eight-bit charge coupled device (CCD) camera coupled with a telecentric lens was used. The working distance was adjusted to 103.5 mm, yielding a conversion factor of 18 $\mu m/pixel$. The shutter time and lighting system were setting to enahnce contrast and avoid under or over exposition. A subset size of 15x15 pixels and a subset step of 13x13 pixels were selected for enhancing spacial resolution. The displacement resolution was in the range of 1-2x10^{-2} pixel depending on the final quality of the speckled pattern. The w_I was then determined by post-procesing the displacement of subsets chosen upper and lower the crack tip during test.

Figura 4: DCB test configuration.

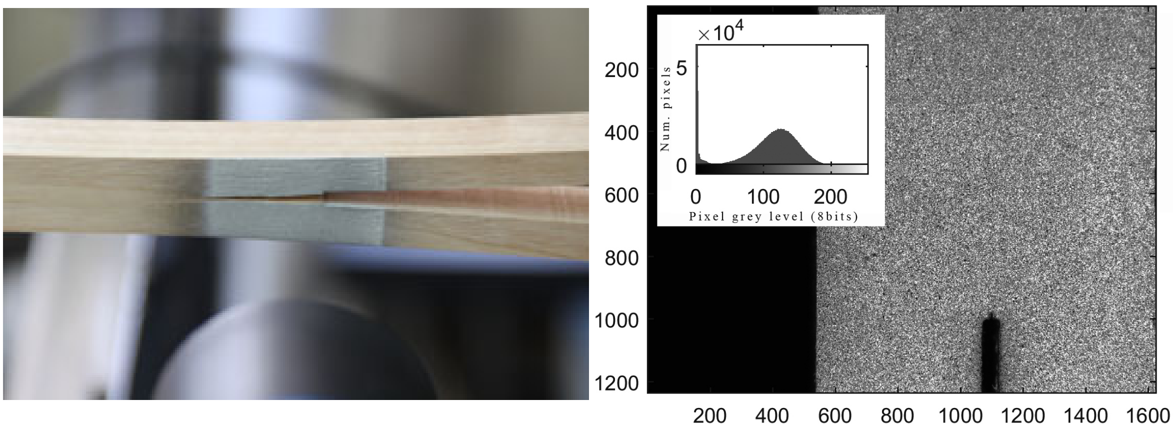

Figura 5: DCB test set-up coupled with DIC.

The evolution of fracture energy in pure mode I (G_I) as a function of the crack length, that is, the resistance curve or R-curve, is determined from the Irwin-Kies formulation (Eq. 18).

$$G_I = \frac{P^2}{2B}\frac{dC}{da} \tag{18}$$

with B denoting the specimen width, and C the compliance obtained directly from the load-displacement curve according to Eq. 19.

$$C = \frac{\delta}{P} \tag{19}$$

As can be seen from Eq. 18, the measurement of the crack length, a, is a fundamental issue. Nevertheless, there are some materials where an accurate direct measurement of this parameter during propagation using standard procedures becomes a difficult task. This is the case of wood, in which a non-negligible fracture process zone (FPZ) ahead of the crack tip is created involving toughening mechanisms like microcracking, crack-branching or fibre-bridging, making difficult the identification of the crack tip. Therefore, the classical data reduction schemes based on a measurements can lead to important errors on the (G_{Ic}) evaluation. In order to overpass this difficulty, the *Compliance-Based Beam Method* (CBBM) [45, 47, 28] was used as data reduction scheme to determine the R-curve from the DCB test, representing a suitable alternative for materials like wood. The CBBM relies on the concept of an equivalent crack length, a_{eq}, and only requires the measurement of the load–displacement ($P-\delta$) curve during the fracture test.

From the Timoshenko beam theory and Castigliano theorem, the compliance of a DCB specimen can be written as shown by Eq. 20:

$$C = \frac{8a^3}{E_L B h^3} + \frac{12a}{5BhG_{LR}} \tag{20}$$

where E_L is the modulus of elasticity in the longitudinal (L) direction and G_{LR}corresponds to the shear modulus in the LR plane. Both values were taking from previous experimental studies carried out by the authors. In Eq. 20 both section rotation and local stress concentration at the crack tip are not considered. In order to take into account these effects and to avoid carrying out additional experimental tests to obtain the elastic properties, the concept of corrected flexural modulus (E_f) was herein proposed. E_f would replace E_L value in Eq. 20 and is determined following Eq. 21 by using the measured initial compliance (C_0) and the corrected initial crack length (a_0 $+\Delta$).

$$E_f = \left[C_0 - \frac{12\,(a_0+\Delta)}{5BhG_{LR}}\right]^{-1} \frac{8\,(a_0+\Delta)^3}{Bh^3} \tag{21}$$

where Δ represents the Williams correction term given by [31] which accounts for the beam root rotation effects at the crack tip. It has the form described in Eqs. 22 and 23).

$$\Delta = h\sqrt{\frac{E_f}{11G_{LR}}\left[3 - 2\left(\frac{\Gamma}{1+\Gamma}\right)^2\right]} \tag{22}$$

$$\Gamma = 1{,}18\frac{\sqrt{E_f E_R}}{G_{LR}} \tag{23}$$

Eqs 21, 22 and 23 can be solved by an iterative procedure until getting a converged value of E_f. In order to consider the FPZ effect at the crack tip during crack propagation, an equivalent crack length ($a_{eq} = a + \Delta + \Delta a_{FPZ}$) instead of a is evaluated from Eq. 20 using Matlab® software [45]. This parameter represents the theoretical crack length to meet the specimen compliance registered during testing. As the current compliance is influenced by FPZ and root rotation effects, these are indirectly considered by using aeq. This procedure has the advantage of taking into account eventual inaccuracies of beam theory and is less sensitive to experimental errors, e.g. initial crack length monitoring and variability of elastic properties.

By combining Eqs. 18 and 20, the strain energy release rate in mode I (G_I) is last obtained (Eq. 24).

$$G_I = \frac{6P^2}{B^2 h}\left(\frac{2a_{eq}^2}{E_f h^2} + \frac{1}{5G_{LR}}\right) \tag{24}$$

By last, the strain energy release rate in mode I (G_I) and CTOD measured by DIC techniques (w_I) can be related by the Eq. 25 [29]:

$$G_I = \int_0^{w_I} \sigma_I(\bar{w}_I)\mathrm{d}\bar{w}_I \tag{25}$$

The cohesive law, $\sigma_I = f\left(w_I\right)$, can be directly obtained by differentiating the previous Eq. 25, leading to Eq. 26:

$$\sigma_I\left(w_I\right) = \frac{\partial G_I}{\partial w_I} \tag{26}$$

This data reduction scheme requires the accurate evaluation of the $G_I = f\left(w_I\right)$relationship. In order to perform the derivative in Eq. 26, the $G_I - w_I$ data can be fitted using continuous approximation funtion described by Eq. 27 (logistic function):

$$G_I = \frac{A_1 - A_2}{1 + \left(w_I/w_{I,0}\right)^p} + A_2 \tag{27}$$

being A_1, A_2, p and $w_{I,0}$constants determined by regression analysis. The A_2 parameter provides an estimation of G_{Ic} in the way: $A_2 = \lim_{w_I \to \infty} G_I = G_{Ic}$. This logistic cohesive law is determined in the present work.

4.2.2. Mode II fracture parameters: End-Notched Flexure test (ENF) method

The ENF was applied to obtain the strain energy release reate in pure mode II (G_{II}) . A schematic representation of this test is shown in Fig. 6. Pre-cracked beam specimens of 500 mm x 20 mm x 20 mm dimensions and 460 mm span were submitted to three-point bending tests inducing a predominant shear loading at the crack tip (Fig. 7). The initial crack length a_0 was about 163 mm, amounting approximately 70 % of mid-span distance in order to ensure stable crack propagation. In the same way as DCB, the ENF tests were carried out in a conventional Instron® testing machine at crosshead displacement rate of 3 mm/min, recording the applied load (P) and the cross-head displacement (δ) with a frequency of 5 Hz during the loading process. The crack tip opening displacemts $(w_{II}$) produced in the vicinity of the crack tip were measured using DIC techniques (Fig. 8).

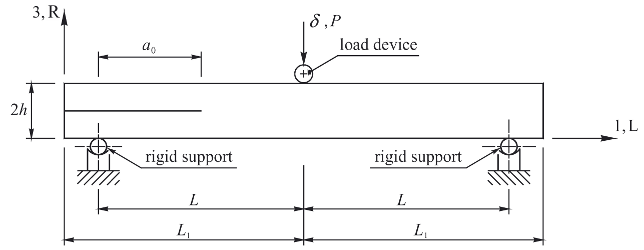

Figura 6: ENF specimen geometry ($2h = 20$ mm, $B = 20$ mm, $2L_1 = 500$ mm, $2L = 460$ mm and $a_0 = 163$ mm).

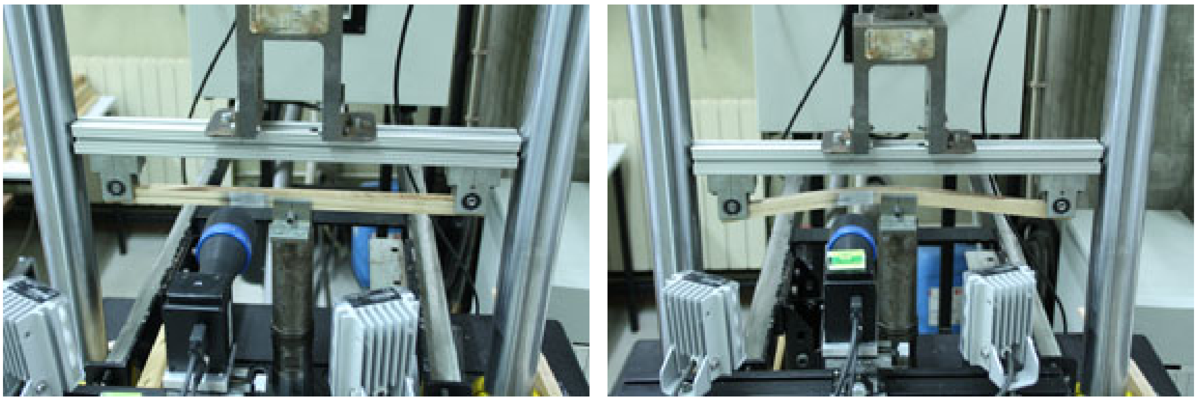

Figura 7: ENF test set-up coupled with DIC.

Similarly to Mode I tests, the CBBM method is appied to Mode II tests as data reduction scheme which is formulated as follows [28, 46].

Assuming the beam theory with shear effects, the specimen compliance during crack propagation can be written as specified in eq. 28.

$$C = \frac{3a_{eq}^3 + 2L^3}{12E_f I} + \frac{3L}{5G_{LR}A} \tag{28}$$

being $e_{eq} = a + \Delta a_{FPZ}$, where Δa_{FPZ} corresponds to the crack length correction accounting for the FPZ effect; $A = 2hB$ describes de cross-section area; and I the second moment of area. It is worth noting that root rotations effects are less important in the ENF configuration compared to DCB. Thus, a specific correction $\Delta$was not taking into account in this case, but rather the root rotation effect is included in the corrected flexural modulus of elasticity which simplifies the method when applied to ENF test and takes the following form (eq. 29):

$$E_f = \frac{3a_0^3 + 2L^3}{12I}\left(C_0 - \frac{3L}{5G_{LR}A}\right)^{-1} \tag{29}$$

where a_0 and C_0 correspond to the initial crack length and initial compliance respectively. During propagation the equivalent crack length can be calculated from eqs. 28 and 29 leading to eq. 30:

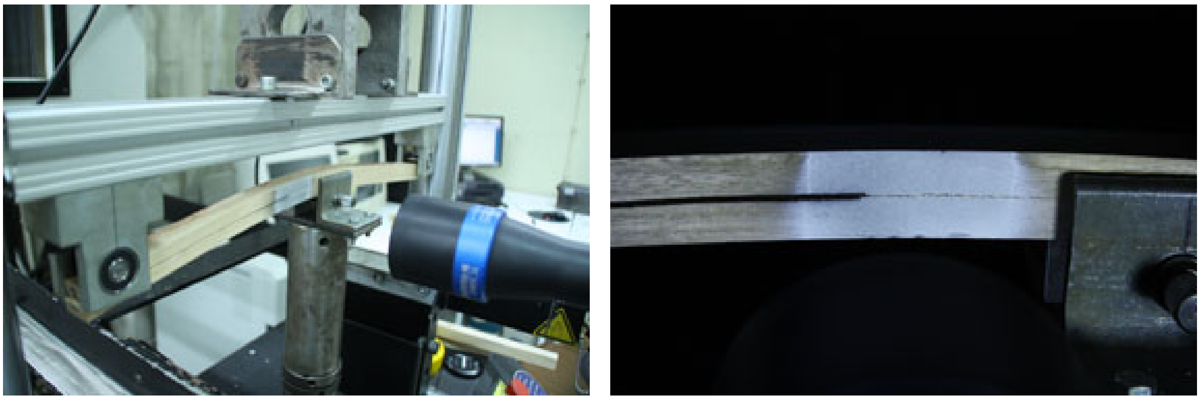

Figura 8: ENF test set-up coupled with DIC.

$$a_{eq} = a + \Delta a_{FPZ} = \left[\frac{C_{corr}}{C_{0corr}} a_0^3 + \frac{2}{3}\left(\frac{C_{corr}}{C_{0corr}} - 1\right) L^3\right]^{1/3} \tag{30}$$

where

$$C_{corr} = C - \frac{3L}{5G_{LR}A} \qquad \text{and} \qquad C_{0corr} = C_0 - \frac{3L}{5G_{LR}A} \tag{31}$$

The critical strain energy release rate, G_{IIc}, can then be calculated applying the Irwin-Kies equation (eq. 18), resulting the expression shown in eq. 32.

$$G_{IIc} = \frac{9P^2}{16B^2 E_f h^3}\left[\frac{C_{corr}}{C_{0corr}} a_0^3 + \frac{2}{3}\left(\frac{C_{corr}}{C_{0corr}} - 1\right) L^3\right]^{2/3} \tag{32}$$

Similarly to DCB tests, the mentioned data reduction method for the ENF studies does not require crack length measurements during propagation since it is based on an equivalent crack concept (eq. 30). Furthermore, a flexural modulus E_f is experimentally determined from the initial compliance C_0avoiding an additional independent test method. Moreover, the CBBM method accounts for the non-negligible energy dissipation which takes place in the FPZ, as this material-weaking process influences specimen compliance.

In a similar way as DCB, the strain energy release rate in mode II (G_{II}) and CTOD measured by DIC techniques (w_{II}) can be related by the Eq. 33 [23]:

$$G_{II} = \int_0^{w_I} \tau_{II}(\bar{w_{II}}) \mathrm{d}\bar{w_{II}} \tag{33}$$

The differentiation of the previous Eq. 33 provides the $\tau_{II} = f\left(w_{II}\right)$ relation (Eq. 34):

$$\sigma_I\left(w_I\right) = \frac{\partial G_{II}}{\partial w_{II}} \tag{34}$$

which represents the cohesive law under mode II loading.

4.2.3. Fracture parameters results

The load-displacement curves obtained from the DCB and ENF tests are shown in Fig. 9.

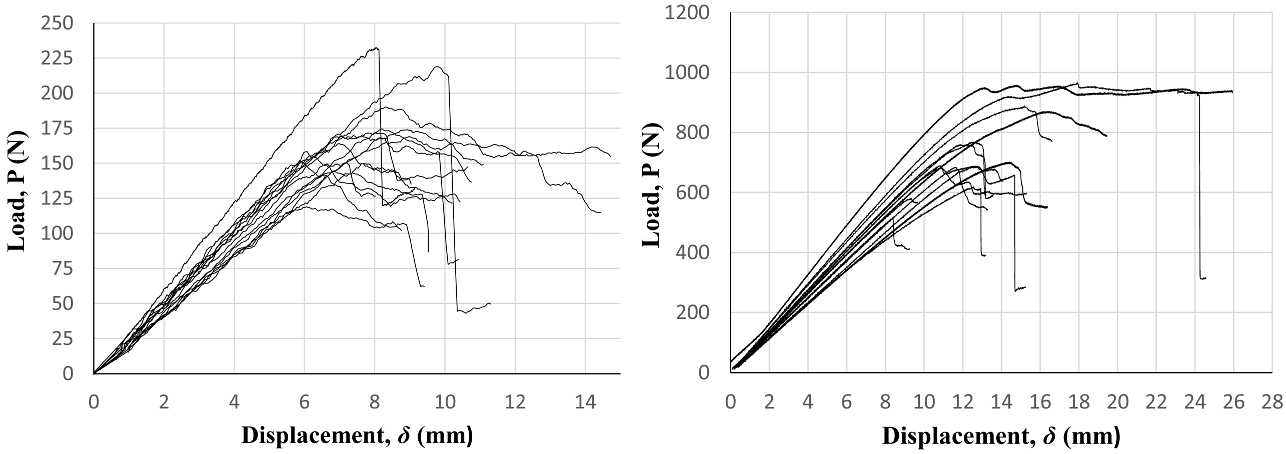

Figura 9: Load-displacement curves of DCB (left) and ENF (right) tests.

The initial compliance C_0 is calculated using Matlab as the result which provides the maximum R^2 in every load-displacement curve. An example of one of the DCB specimens is represented in fig. 10.

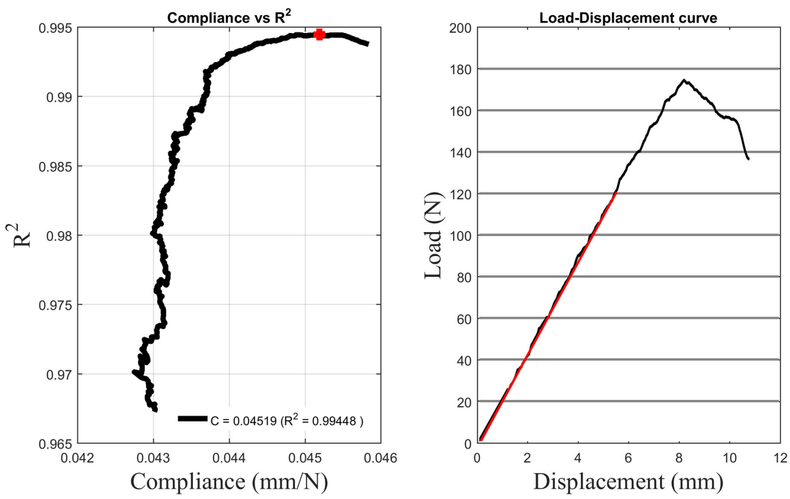

Figura 10: Initial compliance determination.

Both group of curves show quite consistent behaviour with typical variation of wood. The non-linear behaviour observed in the $P - \delta$ curves before the peak reveals that a non-negligible FPZ develops ahead of the crack tip. This phenomenon is a characteristic of quasi-brittle materials as wood, and reflects on pronounced R-curves. The R-curve obtained from DCB tests are shown in Fig.11. From them, following an initial rising domain characterized by the development of the FPZ, the resistance to crack growth tends to a horizontal asymptote which defines the value of fracture energy. In this research most of the specimens provided clear plateaus for a given crack extent allowing the determination of the fracture energy under self-similar crack growth conditions.

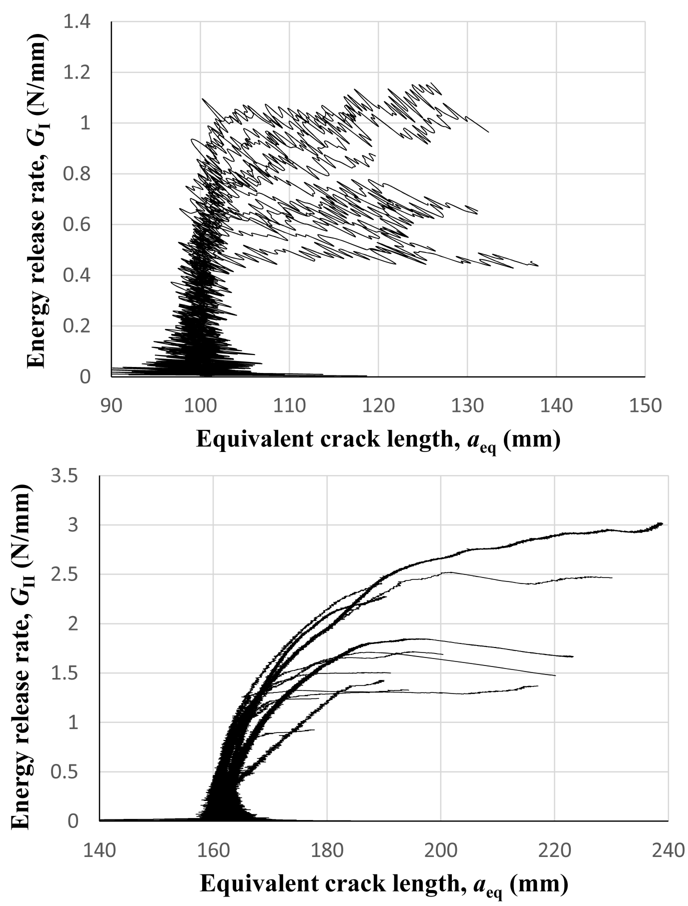

Figura 11: R-curves of all DCB tests (up); R-curves of all ENF tests (down).

Two definitions were chosen for the evaluation of the critical strain energy release rate from the R-curves: (i) $G_{I,P_{max}}$ was considered at the maximum load value and can be taken as a practical measure of the mode I critical strain energy release rate; (ii) G_{Ic} was determined as the mean value over a plateau region of the R-curve as illustrated in Fig. 11. The convergence to a critical strain energy release rate was assessed by the coefficient of variation determined over the value in the plateau of the R-curves. The results for both DCB and ENF tests are sumarized in Tables 3 and 4 respectively together with the máximum load reached in every test and initial compliance.

Tabla 3: Fracture energy obtained from DCB specimens by means of CBBM.

Specimen ref.	P_{max}[N]	C_0[mm/N]	$G_{I,P_{max}}$[N/mm]	G_{Ic}[N/mm]
140-1	191.70	0.042	1.07	1.01
144-1	173.00	0.040	0.81	0.84
144-2	123.08	0.048	0.52	0.48
161-1	172.35	0.047	0.97	0.95
161-3	176.29	0.040	0.85	0.85
176-1	151.70	0.042	0.65	0.61
176-2	156.59	0.049	0.82	0.76
176-3	183.95	0.048	1.10	1.02
189-1	168.16	0.040	0.75	0.70
189-2	177.06	0.045	0.95	0.92
192-1	162.01	0.038	0.65	0.63
192.2	147.76	0.043	0.70	0.65
192-3	153.99	0.038	0.56	0.57
average	164.43	0.043	0.80	0.77
SD	18.03	0.004	0.18	0.18
CoV [%]	11	9	23	23

Tabla 4: Fracture energy obtained from ENF specimens by means of CBBM.

Specimen ref.	P_{max}[N]	C_0[mm/N]	$G_{II,P_{max}}$[N/mm]	G_{IIc}[N/mm]
140-1	958.30	0.012	2.14	2.17
144-1	888.31	0.014	2.42	2.50
144-2	701.22	0.018	1.79	1.84
144-3	618.65	0.017	1.37	1.38
161-1	870.21	0.015	2.48	2.60
161-2	798.87	0.015	1.63	1.70
176-1	756.00	0.016	1.27	1.32
176-2	577.72	0.016	0.69	0.70
176-3	688.20	0.017	1.46	1.50
189-1	966.24	0.014	2.21	2.40
189-2	756.67	0.015	1.18	1.24
189-3	727.30	0.015	0.88	0.90
192-1	684.18	0.015	1.24	1.28
192.2	761.13	0.015	1.51	1.70
average	768.07	0.015	1.61	1.66
SD	117.58	0.001	0.58	0.59
CoV [%]	15	10	36	35

From post-processing the displacements provided by DIC measurements, both normal and transverse CTOD with regard to the crack plane were determined during DCB and ENF tests as shown in Fig. 12. As expected, CTOD in mode II (w_{II}) was negligible in DCB mode I tests. The opposite is happened when ENF are studied, although in this case w_I is not entirely negligible.

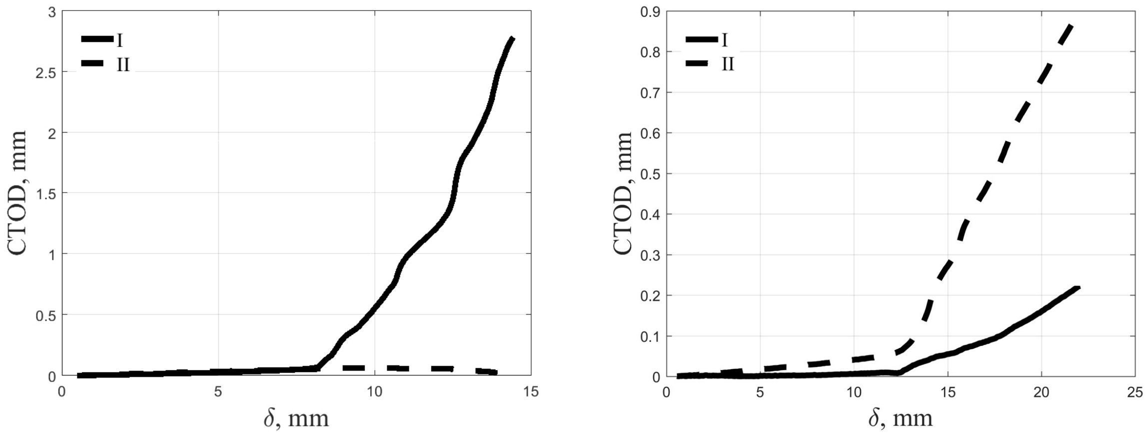

Figura 12: Normal and transversal CTOD for a representative DCB (left) and ENF (right) tests.

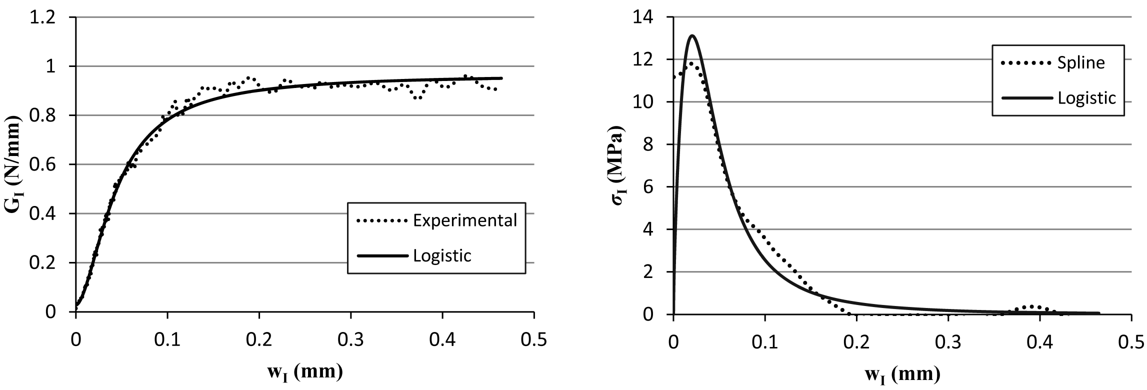

Figura 13: Characteristic $G_I - w_I$ and regression with the logistic function (left) and logistic and spline cohesive law (right) for a representative DCB test.

Characteristic $G - w$ curves where then obtained as shown in Fig. 13 (left). The cohesive law was finally determined by fitting a logistic function to the experimental data as is represented in Fig. 13 (right).

4.3. Connection tests

An experimental program of dowel-type connections loaded perpendicular to grain is presented in this section. Series with one dowel and two dowels in a row and different loaded edges distances are conducted.

In addition, the adequacy of the different analytical models compiled in section 3 to the experimental data obtained for ecualyptus is here discussed.

4.3.1. Method

Splitting tests were conducted on *Eucalyptus globulus* beams of 29 x 116 mm^2 cross-section, 580 mm length and 500 mm span. This cross-section is limited by the available dimensions of the sawn material.

The beams were loaded at midspan in three-point bending setups (fig. 14). Different configurations following three different edge distances, $h_e = 4d$, $h_e = 3d$, and $h_e = 2d$, using a single steel dowel of $d = 16$ mm diameter and 4.2 quality were studied. It must be noted that $h_e = 4d$ corresponds to the minimum edge distance established in Eurocode 5 to try to eliminate the risk of brittle splitting failures. $h_e = 3d$, and $h_e = 2d$ were tested in order to analyze a possible section optimization in this species and also to understand better the splitting behaviour. These configurations correspond to $\alpha = h_e/h$ values of 0.55, 0.41 and 0.27 respectively (test data included in literature have shown that α values up to 0.7 fail by splitting [38]). Between seven and nine replicates were tested for each configuration.

When testing edge distances larger than $4d$, a single dowel often causes significant embedment, in which case two closely spaced dowels could be used in order to increase the bearing area. Two closely spaced dowels are known to give almost the same splitting failure load as a single dowel [41, 36]. Therefore, beam configurations using two steel dowels of $d = 16$ mm diameter aligned along the grain and separated $3d$ distance between their centers were prepared (fig. 14). Eight replicates with an edge distance of $h_e = 4d$ was considered for this configuration.

The tests were carried out in a conventional Instron® testing machine at crosshead displacement rate in the range of 0.5-2 mm/min in order to reach failure in around 5 min (for one single dowel configuration,$h_e = 4d$ beams were tested at 2 mm/min velocity; $h_e = 3d$ beams at 1 mm/min; and $h_e = 2d$ beams at 0.5 mm/min; $h_e = 4d$ beams with two dowels were tested under 0.7 mm/min velocity). The dowels were loaded by two outer plates made of Eucalyptus globulus with similar characteristics as the beams (it must be noted that no embedment damage were produced at the plates). During the loading process, the applied load (P) and the displacement (δ) were recorded. For the latter two strain gauges were used: one located at the middle bottom side of the specimen and the other one on the steel dowel (Fig. 15).

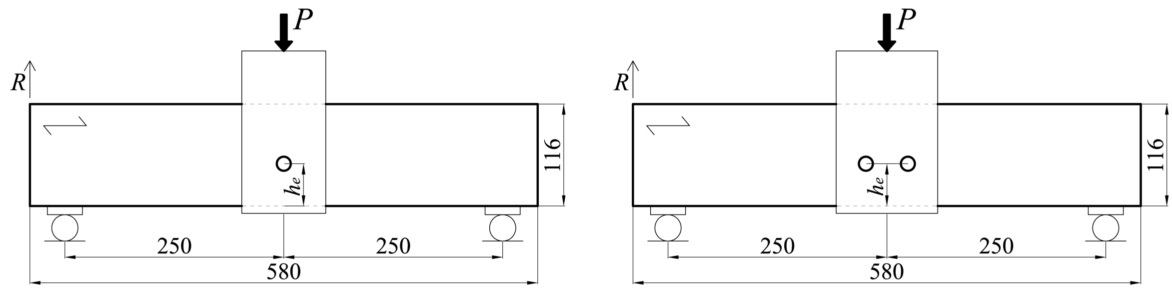

Figura 14: Single-dowel (left) and double-dowel (right) connection geometry.

Figura 15: Single-dowel connection test.

4.3.2. Results

From the single-connection tests, a main crack growing from both sides of the dowel could always be observed (Fig.16). This crack develops on slightly different positions starting at the mid-down part of the dowel contact. The smaller the loaded edge distance, the faster the crack growths in respect to the maximum load capacity. In these group of tests the crack never reached the beam ends. In terms of ductile behavior, small embedding deformations under the dowels but no bending of the dowels could be observed in some of the specimens with higher loaded edge distance $4d$ as well as some cracks with small lengths beside the dowel (Fig. 17). The specimens of *2d* and *3d* edge distances did not show any important embedment under the dowels. In any case, the brittle failure is always characterized by one main crack.

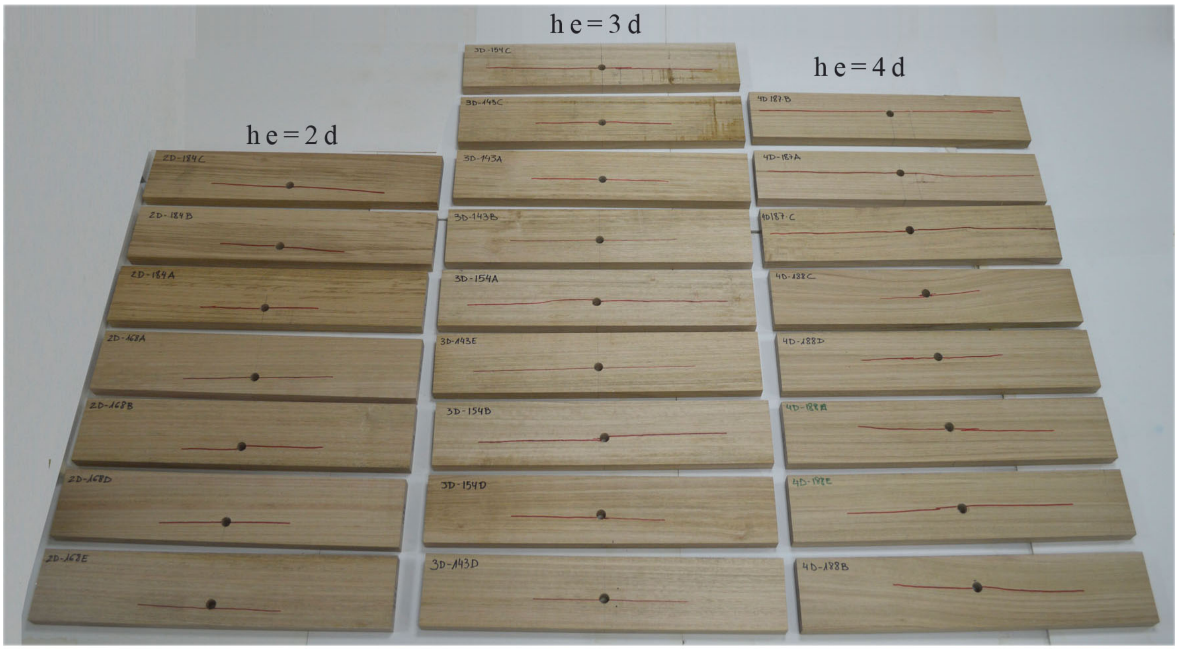

Figura 16: Tested single-dowel specimens. From left to right: *2d*, *3d* and *4d* edge distances series.

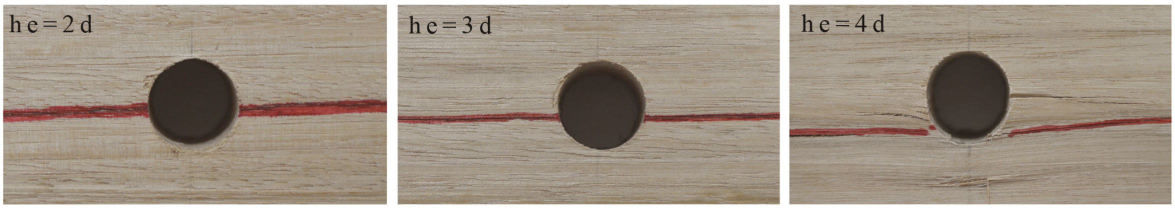

Figura 17: Detail of the local failure around the dowel for the three edge distances.

The double-dowel test series show a crack growing process similar as that of single-dowel one in terms that just one main crack grows to both sides of the beam. Nevertheless, in all these specimens the crack reached the beam ends dividing them into two parts with a very brittle and sudden failure (figs. 18 and 19). No embedding deformations under the dowels were observed.

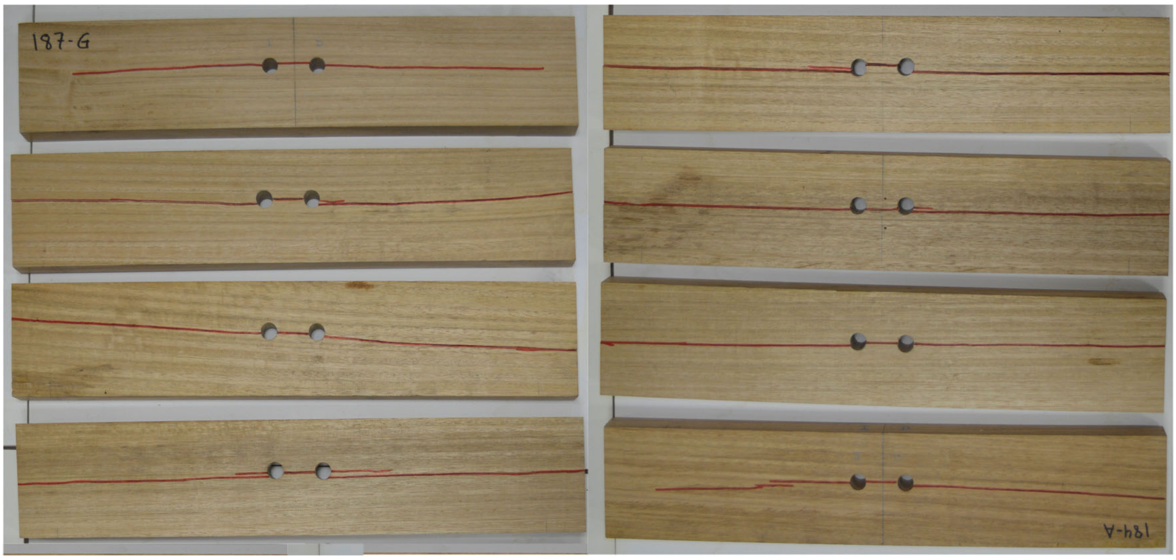

Figura 18: Tested double-dowel specimens.

Figura 19: Typical failure behaviour of double-dowel test series (left); detail of the local failure around the dowels (right).

These failure modes are well represented by the load-displacement curves shown in Fig. 20

for both single and double-dowel series of tests.

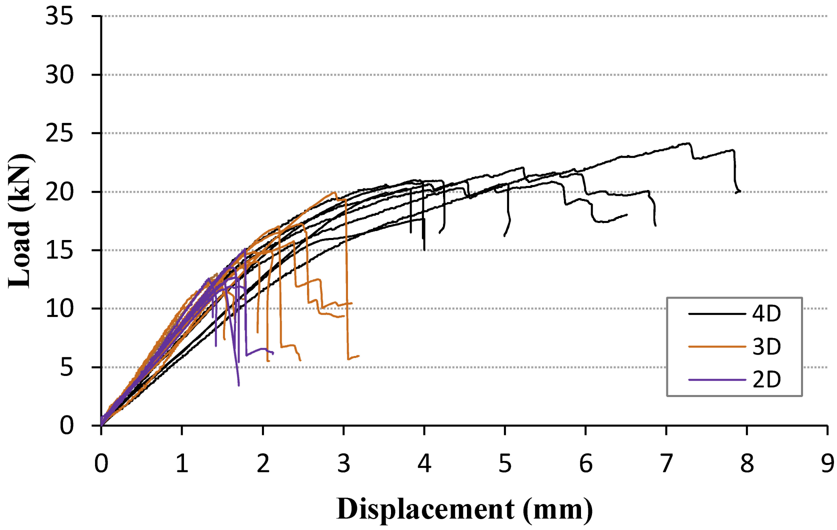

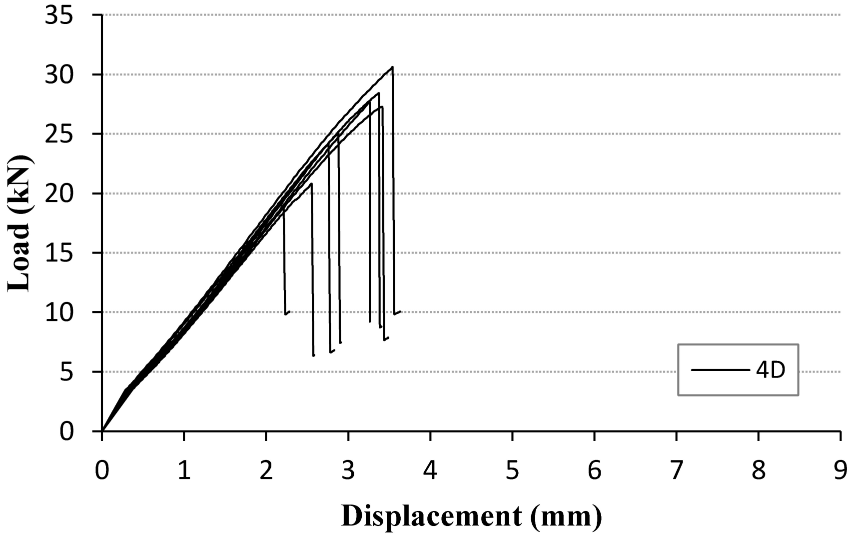

Figura 20: Load-displacement curves from single-dowel (up) and double-dowel (down) splitting tests.

The failure loads of the tested beam specimens are shown in Table 5.

The results reflects the different failure behaviour of the connection layouts investigated.

In the case of a single-dowel, the load capacity increases for the same connection layout with increasing the load edge distance. The load-displacement curves show a ductile behaviour for the greater edge distance (*4d*), characterized by embedment stresses and yielding followed by hardening. The connection still is able to force splitting failure after considerable slip although splitting is not the primary failure mode. On the contrary, a brittle failure response is displayed for lower edge distances *3d* and *2d*. Therefore, applying the minimum limitation of $h_e = 4d$ established in the European standard to eliminate the risk of splitting failure in softwoods seems to lead to a safe situation for eucalyptus.

Tabla 5: Failure loads of the connection tests.

1 dowel			2 dowels		
h_e [mm]	Specimen	P_u [kN]	h_e [mm]	Specimen	P_u [kN]
$2d = 32$	168a	12.30			
	168b	12.57			
	168d	13.46			
	168e	12.67			
	184a	11.21			
	184b	11.88			
	184c	15.09			
	mean	**12.74**			
$3d = 48$	143a	12.68			
	143b	13.96			
	143c	13.92			
	143d	12.55			
	143e	14.87			
	154a	19.88			
	154b	17.24			
	154c	16.99			
	154d	15.74			
	mean	**15.31**			
$4d = 64$	188a	22.05	$4d = 64$	183a	20.80
	188b	20.87		183b	28.42
	188c	24.13		183c	24.18
	188d	21.00		183d	27.25
	188e	20.85		183e	30.61
	187a	20.24		184a	27.65
	187b	17.64		187f	25.12
	187c	20.74		187g	18.90
	mean	**20.94**		**mean**	**25.37**

The test serie with two-dowels placed in a row parallel to grain lead to slightly higher failure loads compared to the single-dowel connection with the same edge distance. A complete and brittle separation of the specimen in two halfs is produced when the ultimate load is reached. Therefore, to avoid a high risk of splitting failure of connections loaded perpendicular to grain when two horizontal dowels are envisioned, the loaded edge distance of *4d* stablished in the Eurocode should be increased for eucalyptus. A further experimental research with higher edge distances for this species and foreseeably for other hardwoods bemoces therefore necessary.

Comparison of theoretical to experimental failure loads

The theoretical capacity strengths for a single dowel connection predicted by the seven different analytical models compiled in section 3 were calculated. The Mode I fracture energy for each specimen determined experimentally (Table 3) and the average shear modulus of the material (Table 1) were used as input parameters in all the models. The average modulus of elasticity (Table 3) was used as input for the four models described with Eqs. 3, 2, 10-12 and 13-14. The tension strength perpendicular to grain was used as input parameter for the lattest two models described with Eqs. 10-12 and 13-14.

The ratios of the theoretically predicted failure loads to the experimental main values for single connection layout are presented in Table 6. These ratios normalize the strength estimates allowing for easier comparison. Ratio < 1 represents a conservatively predicted connection strength; ratio$\approx$1 means an accurately predicted connection strength; and ratio > 1 depicts an overpredicted connection strength.

Tabla 6: Theoretical to experimental failure loads ratios from single-dowel connection tests.

h_e [mm]	Specimen	Eq. 3	Eq. 4	Eq. 2	Eqs. 6-7	Eq 8	Eqs. 10-12	Eqs. 13-14
$2d = 32$	168a	1.33	1.33	1.55	1.55	1.34	1.12	1.31
	168b	1.30	1.30	1.52	1.52	1.31	1.10	1.28
	168d	1.21	1.21	1.42	1.42	1.22	1.02	1.20
	168e	1.29	1.29	1.51	1.51	1.30	1.09	1.27
	184a	1.46	1.46	1.70	1.70	1.47	1.22	1.43
	184b	1.37	1.37	1.61	1.61	1.39	1.15	1.35
	184c	1.08	1.08	1.26	1.26	1.09	0.91	1.06
$3d = 48$	143a	1.58	1.58	2.06	2.06	1.63	1.38	1.81
	143b	1.43	1.43	1.87	1.87	1.48	1.26	1.64
	143c	1.43	1.43	1.87	1.87	1.49	1.26	1.64
	143d	1.59	1.59	2.08	2.08	1.65	1.40	1.82
	143e	1.34	1.34	1.75	1.75	1.39	1.18	1.54
	154a	1.00	1.00	1.31	1.31	1.04	0.87	1.14
	154b	1.16	1.16	1.51	1.51	1.20	1.01	1.32
	154c	1.18	1.18	1.54	1.54	1.22	1.02	1.34
	154d	1.27	1.27	1.66	1.66	1.32	1.10	1.44
$4d = 64$	188a	1.05	1.05	1.56	1.56	1.15	0.94	1.40
	188b	1.11	1.11	1.65	1.65	1.21	0.99	1.48
	188c	0.96	0.96	1.43	1.43	1.05	0.86	1.28
	188d	1.10	1.10	1.64	1.64	1.20	0.98	1.47
	188e	1.11	1.11	1.65	1.65	1.21	0.99	1.48
	187a	1.14	1.14	1.70	1.70	1.25	1.02	1.52
	187b	1.31	1.31	1.95	1.95	1.43	1.16	1.74
	187c	1.11	1.11	1.66	1.66	1.22	0.99	1.48

Fig. 21 shows graphically the aforementioned failure load ratios for the single-dowel connection. The results from the $h_e = 2d$ specimens are represented in red, from $h_e = 3d$ in blue and from $h_e = 4d$ in green. Every symbol corresponds to an analytical model equation.

As can be derived from the Table 6 and Fig. 21, most of the analytical models overpredict the splitting capacity for single-dowel specimens of eucalyptus.

The models given by Eqs. 2 and 6-7 produce the worst predictions in single-dowel specimens (it must be noted that Eq. 6-7 is the base of the Eurocode 5 splitting formula). As the experimental value of fracture energy is directly used in these equations, it seems to suggest

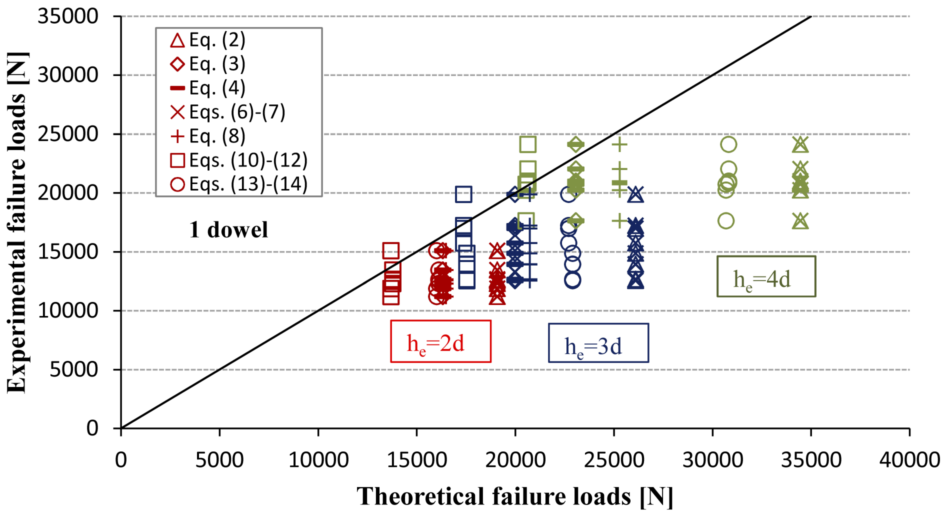

Figura 21: Single-dowel tests: experimental failure loads versus theoretical failure loads from the analytical models presented in section 3.

that the linear fracture mechanics model on which these equations are based may contain some deficiencies. It is also in agreement with the results obtained by Jensen *et al.* (2015) [36] for LVL specimens made of Radiata pine.

The models given by Eqs. 3 and 4 show better predictions than Eqs. 2 and 6-7 noting than the former are just special cases of the latter (see section 3). In any case, all of them show the same trend.

Eqs. 10-12 led to the best predictions bringing them successfully in better agreement with the experimental results. These results are similar to the findings by Hindman *et al.* (2010) [20] and Patel and Hindman (2012) [44] who concluded that Eqs. 10-12 performed better than Eqs. 6-7 for MSR, LVL and PSL. Differences between Eqs. 10-12 and other of the considered models could be related to the inclusion of the tension perpendicular to grain strength of the member. In addition, the splitting failure load is not proportional to the square root of the fracture energy. Therefore, the solutions can not be enclosed within linear elastic fracture mechanics (LEFM). They belong to the quasi-nonlinear fracture mechanics, and the LEFM solutions described by Eqs. 13-14 are considered as special cases from it which result in predictions less close.

In the same way, the ratios of the theoretically predicted failure loads to the experimental main values for double-dowel connection specimens are presented in Table 7Fig. 22 shows the failure load ratios for the double-dowel connections. As can be seen, Eqs. 10-12, 3 and 4 give the best predictions as happened for single-dowel connections. In these cases, a greater amount of specimens provide ratios below 1 which would represent a conservatively predicted splitting load.

Tabla 7: Theoretical to experimental failure loads ratios from double-dowel connection tests.

h_e [mm]	Specimen	Eq. 3	Eq. 4	Eq. 2	Eqs. 6-7	Eq 8	Eqs. 10-12	Eqs. 13-14
$4d = 64$	183a	1.11	1.11	1.66	1.66	1.59	0.98	1.47
	183b	0.81	0.81	1.21	1.21	1.17	0.72	1.08
	183c	0.95	0.95	1.42	1.42	1.37	0.85	1.27
	183d	0.85	0.85	1.26	1.26	1.22	0.75	1.12
	183e	0.75	0.75	1.13	1.13	1.08	0.67	1.00
	184a	0.83	0.83	1.25	1.25	1.20	0.74	1.11
	187f	0.92	0.92	1.37	1.37	1.32	0.82	1.22
	187g	1.22	1.22	1.82	1.82	1.75	1.09	1.62

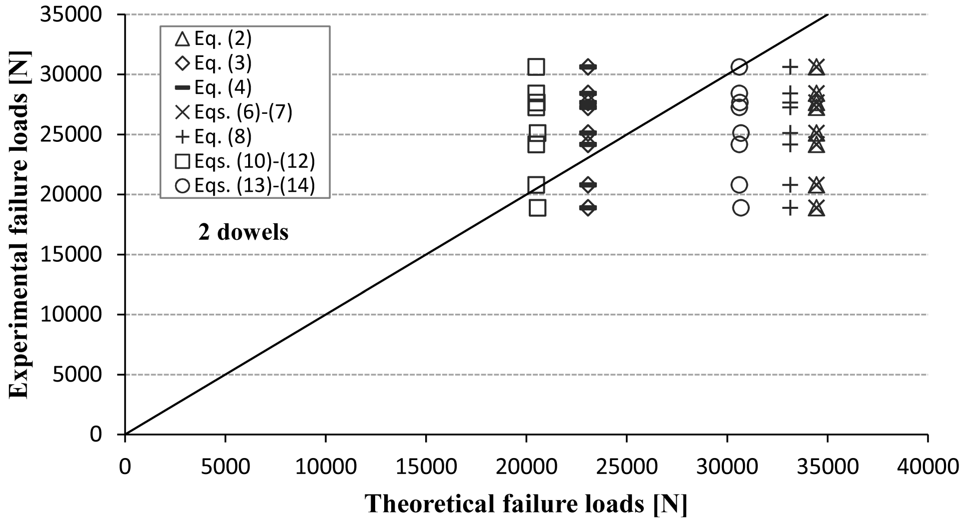

Figura 22: Double-dowel tests: experimental failure loads versus theoretical failure loads from the analytical models presented in section 3.

Design value comparison

As mentioned in section 3, a manifestation of the analytical equation 6 referred previously appears in the Eurocode 5 as specific check of the splitting capacity for perpendicular-to-grain connections in softwoods. It originates from a LEFM approach proposed by Van der Put (2000) [54] based on assumptions of a single and infinitely stiff dowel which is symmetrically loaded with respect to the wood member width:

$$F_{90,Rk} = bC_1\sqrt{\frac{h_e}{1-\frac{h_e}{h}}} \tag{35}$$

The factor C_1 depends on what is known as *apparent fracture parameter*, $\sqrt{GG_c}$, representing the square root of the shear modulus times critical energy release rate in the form:

$$C_1 = \sqrt{\frac{GG_c}{0{,}6}} \tag{36}$$

The model was calibrated by Van der Put using $\sqrt{GG_c}$ as a fitting parameter taking test data from a limited number of sources with different type of connection. The mean lower bound of the apparent fracture parameter $\sqrt{GG_c} = 12\,N/mm^{1,5}$ was selected, which leads to a factor $C_1 = \sqrt{\frac{GG_c}{0{,}6}} = 15{,}5\,N/mm^{1,5}$. In order to derive a characteristic value, the C_1 factor was further reduced to $15{,}5 \cdot 2/3 \approx 10\,N/mm^{1,5}$, and this value was suggested to be used for the code design criterion.

Even so, the value finally adopted by the Eurocode 5 is for all the softwoods is $C_1 = 14\,N/mm^{1,5}$ which corresponds to an apparent fracture parameter of $\sqrt{GG_c} = 10{,}84\,N/mm^{1,5}$ $\left(= 14\sqrt{0{,}6}\right)$.

Proceeding in a similar way as mentioned above, the value of C_1 factor of the Eurocode 5 formula which would correctly predict the experimental failure loads obtained for eucalyptus is derived (Table 8). As can be seen, the lower characteristic value of C_1 factor (calculated as $2/3C_1$) results in **19.45** $N/mm^{1,5}$, which is 1.39 times the value established by the Eurocode 5 for softwoods ($C_1 = 14\,\mathrm{N/mm}^{1,5}$), which seems to be conservative for hardwoods.

Tabla 8: C_1factor according to Eurocode 5.

h_e [mm]	$\sqrt{GG_c}$ $[N/mm^{1,5}]$ (mean)	C_1 $[N/mm^{1,5}]$ (mean)	C_1 $[N/mm^{1,5}]$ (characteristic)
		1 dowel	
$2d = 32$	25.72	33.20	22.13
$3d = 48$	22.60	29.18	**19.45**
$4d = 64$	23.40	30.21	20.14
		2 dowels	
$4d = 64$	28.35	36.60	20.40

Eurocode 5 design values were also calculated according to Eq. 17 being $C_1 = 14\,\mathrm{N/mm}^{1,5}$ and are presented in Table 9. The design capacity does hence not explicitly depend on any material parameters, and is valid just for softwoods with no consideration to hardwoods or any other wood-based material. For the connection case studied in the present work, loaded edge distance and beam depth are therefore the only two input parameters needed to calculate the splitting capacity. Values were adjusted to the design values accounting for the material type, load duration and moisture content effects ($k_{mod} = 0{,}9$ and $\gamma_M = 1{,}3$). The averages and COVs values of the design factor of safety (DFS) for each configuration defined as the ratio of the test capacity strength to the Eurocode 5 design splitting capacity are also included in Table 9.

Tabla 9: Splitting capacities according to Eurocode 5 and design factors of safety.

h_e [mm]	$F_{90,Rk}$[N]	$F_{90,Rd}$[N]	DFS (mean)	COV (%)
		1 dowel		
$2d = 32$	2686.1	1859.6	3.4	9.8
$3d = 48$	3673.8	2543.4	3.0	15.7
$4d = 64$	4851.1	3358.5	3.1	8.6
		2 dowels		
$4d = 64$	4851.1	3358.5	3.8	15.6

Values of DFS generally ranged from 2.5 to 4.6 with no distinct trend with respect to the load edge distance. Therefore, the prediction formula included in the Eurocode 5 is prone to underestimate splitting capacity of the specimens leading to high conservative predictions.

Nevertheless, when the mean G and G_c values obtained from the experimental tests with Eucalyptus globulus are considered (G_{LR} = 1926 N/mm^2 and G_{Ic} = 0,77 N/mm respectively), the apparent fracture parameter $\sqrt{GG_c}$ results in 38.51 $N/mm^{1,5}$. It leads to a C_1 = 49,71 N/mm^{1,5} , which can be reduced by 2/3 obtaining the characteristic value of **33.14** $N/mm^{1,5}$, 2.37 times the value stablished by the Eurocode 5 and higher than the value obtained from the process shown in Table 8.

In summary, these results indicate that the analytical model on which the Eurocode 5 is based overpredicts the splitting capacity of the connection when the real fracture parameters of the material are considered. This fact could lead to a dangerous design situation. On the other hand, the formula included in the Eurocode 5 (with a fixed value of $C_1 = 14\,\text{N/mm}^{1,5}$) results to be very conservative for this species. Therefore, as demostrated in the previous section, the analytical model base of the Eurocode 5 does not bring good predictions for eucalyptus, and so require a review for any specific hardwood. Analytical models including the tension perpendicular to grain strength of the member led to better agreement with the experimental results.

5. Numerical research

In this section, a 2D numerical modeling of the single-dowel type connections with different edge distances loaded perendicular to the grain is shown. The results are compared to the experimental values for ecualyptus presented in section 4.3. The model is developed using the finite element sofware ANSYS 17.1.

5.1. Model definition

The connection geometry and dimensions correspond to the specimens used in the experimental study. The connection position is placed at midspan of the beam with three different loaded edge distances according to the experimental research: $h_e = 4d$, $h_e = 3d$ and $h_e = 2d$, being d=16 mm the dowel diameter.

The *Eucalyptus globulus* material is defined using quadratic eight-node elements (PLANE183). The orthotropic coefficients required for their implementation in the model were determined in advance in previous experimental campaigns with galician *Eucalyptus globulus* of similar density as the boards used in the present fracture and connection tests. The values were shown in Table 2.

The steel material of the dowel and the bearing plates of the supports are considered as isotropic with $E = 210000\,N/mm^2$ and υ = 0,3, and modeled using quadratic eight-node plane elements (PLANE183). The friction coefficient considered between the wooden beam and steel dowel and bearing plates is set to 0.6 according to literature.[15].

As could be seen in the experimental results, multiple cracks with small lengths beside the dowels were show at the beginning of the tests just in the case of the higher load edge distance $4d$, but just one main crack always characterized the brittle failure. This brittle failure behaviour can be implemented in ANSYS by using the cohesive zone model [24], in which three-node surface to surface contact elements are located along the critical areas of the specimen. The element pairs are separated according to the defined cohesive zone material law depending on the stress-strain distribution and thus create new surfaces comparable to realistic crack propagation. The cohesive zone material available in ANSYS for Mode I of fracture is defined by three parameters: the normal contact stiffness, K_n, corresponding to the elasticity modulus in the applied direction; the maximum tension strength perpendicular to the grain, $f_{t,90}$; and the critical fracture energy in Mode I, G_{Ic}. The cohesive law is simplified as a bilinear relationship as shown in fig. 23-left, where u_n denotes the normal contact gap and d_n the debonding parameter, the latter being zero until maximum $f_{t,90}$. The complete separation of the contact element pair occurs at u_n^c contact gap.

The Mode II of fracture is also implemented in ANSYS analogously to Mode I, by considering the tangential constant stiffness, K_t; the shear strength, f_v; and the critical fracture energy for Mode II, G_{IIc}, and following an equivalent bilinear behaviour.

The Mixed Mode is defined by eq. 37:

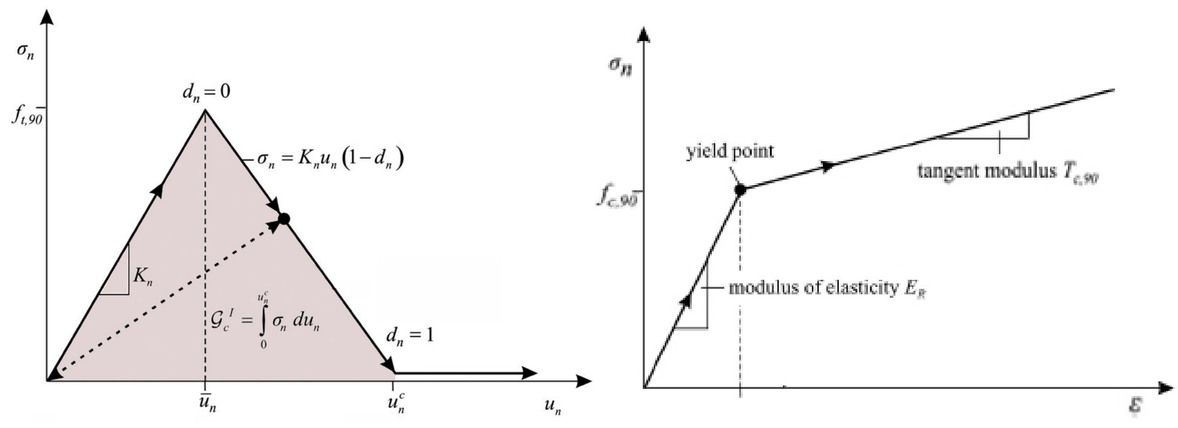

Figura 23: Bilinear cohesive law for brittle fracture Mode I (left); ductile behaviour of wood under compression (right).

$$\frac{G_I}{G_{Ic}} + \frac{G_{II}}{G_{IIc}} = 1 \tag{37}$$

According to that, a layer of contact elements oriented parallel to the grain and placed at both sides of the dowel were used to simulate the crack paths which form the cohesive zones in the connection numerical model (fig. 24). The layer consists on quadratic three-node surface-to-surface contact element pairs (CONTA172 and TARGE169) with the cohesive zone parameters for Mixed Mode I and II determined in the experimental campaign included in section 4.2:G_{Ic} = 0,77 (N/mm) and G_{IIc} = 1,66 (N/mm) respectively; and the tension and shear strengths obtained from previous studies for this material: $f_{t,90}$ = 7,5 (N/mm^2) and f_v = 16,2 (N/mm^2)

In addition to the brittle behaviour, for the specimens with $h_e = 4d$ also the ductile failure behaviour under compresion perpendicular to grain is modelled considering a bilinear elastic-plastic material with isotropic hardening after yielding together with the application of the anisotropic Hill theory (fig. 23 right). It is available in Ansys as BISO material and HILL coefficients. The tanget modulus and yielding strength needed to define such law are considered as 3 (N/mm^2) and 30 (N/mm^2).

As the results showed a similar behaviour with five layers of cohesives than with one layer placed in the middle-height of the dowel, the latter configuration was followed in order to save time in computation. This is also in accordance to the study carried out by [15].

The model mesh is shown in Fig. 24.

5.2. Results

Fig. 25 represents the typical deformed shape from a $4d$ edge distance model when the failure is totally developed.

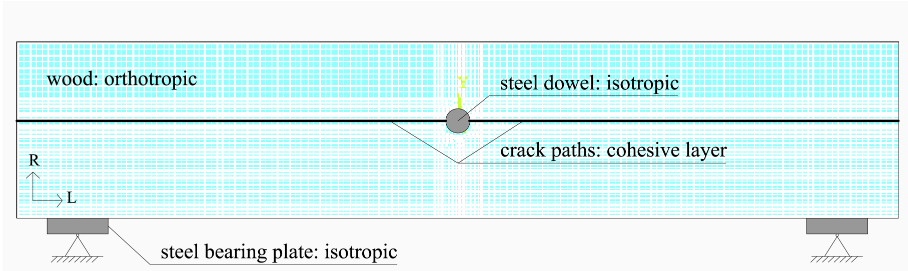

Figura 24: Meshing of the numerical model

Some details of the dowel zone at a displacement of around 1.6 mm are shown in Fig. 26 for the three different configuration of edge distances. As can be seen, the crack has already developed in the two more brittle configurations, whereas specimens with $4d$ show mostly embedding under the dowel.

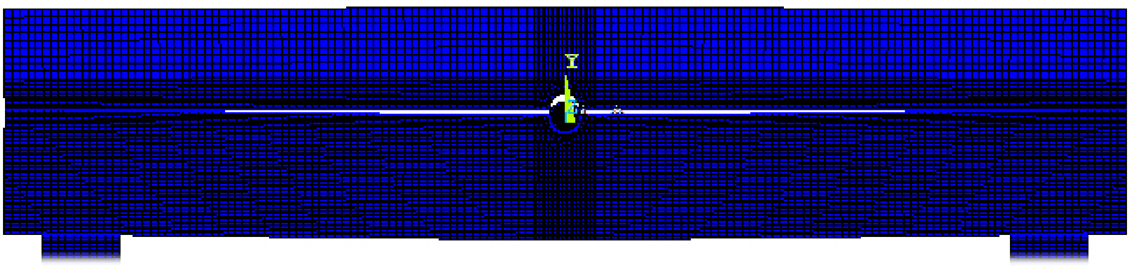

Figura 25: Typical deformed shape.

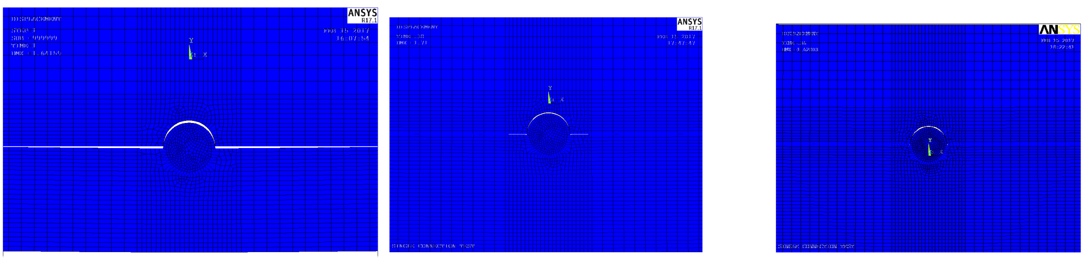

Figura 26: Failure detail at 1.6 mm displacement. From left to right: *2d*, *3d* and *4d* edge distances.

The numerical load-deflection curves obtained for the three edge distances layouts compared with the experimental ones are shown in Fig. 28 for the three edge distance configurations. Great similarities between numerical and tests results in terms of the linear elastic and softening behaviours can be observed. The numerical ultimate failure load results close to the highest experimental values. The initial stiffness is also sligthly higher than those despicted by some of the experimental tests. It could be due to possible dowel deformations that are difficult to measure considering the loading device. In any case, this deformation difference is of small amount as can be observed in the figures. Nonetheless, the model is planned to be improved in further research as it was just a first closeness to it.

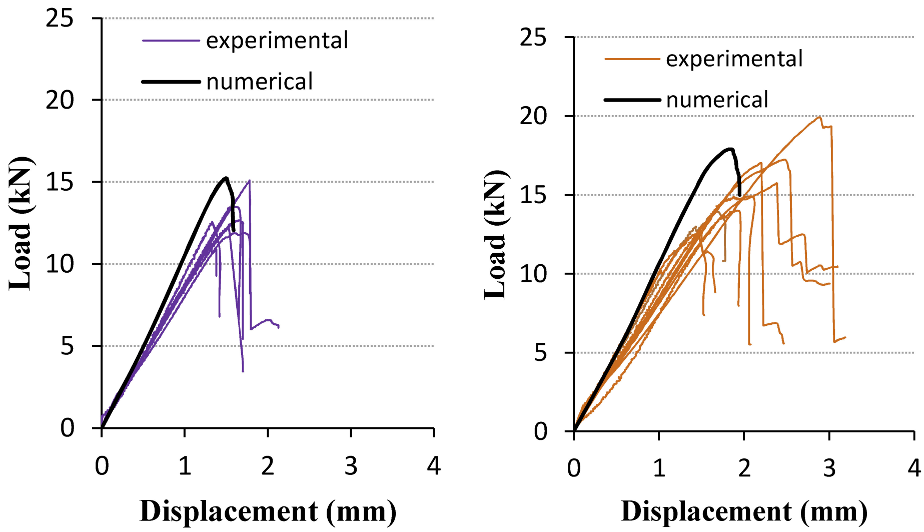

Figura 27: Experimental and numerical load-deflection curves from *2d* (left) and *3d* (right) edge distances layouts.

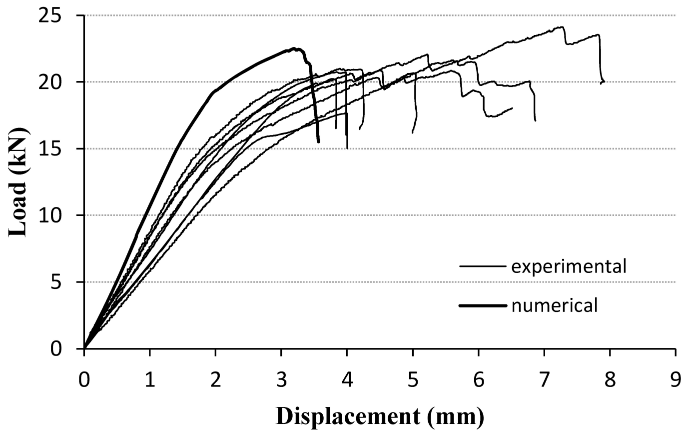

Figura 28: Experimental and numerical load-deflection curves from *4d* edge distances layout.

6. Conclusions

The main intention of this STSM at Univerity of Trás-os-Montes e Alto Douro was to gain deeper knowledge regarding the splitting capacity of hardwoods connections loaded perpendicular to grain as no equation for its prediction is included in the Eurocode 5 (just for softwoods).

With this aim, splitting tests were conducted on beams made of Eucalyptus globulus loaded by single-dowel connections with three different loaded edge distances ($h_e = 4d$, $h_e = 3d$ and $h_e = 2d$); and by double-dowel connections positioned in a row at $h_e = 4d$. The minimum loaded edge distance $4d$ established in the Eurocode 5 to try to eliminate the risk of brittle splitting failure seems to be valid for Eucalyptus globulus just in the case of single-dowel connections beams. On the contrary, all the specimens with double-dowel connections positioned at $h_e = 4d$ showed sudden brittle failures at sligthly higher ultimate loads than those reached by the single-dowel tests for the same loaded edge distance. Therefore, further experimental research for this species and foreseeably for other hardwoods bemoces necessary to increase the minimum $4d$ edge distance stablished in the Eurocode 5 when two dowels in row are envisioned.

Also the applicability to eucalyptus of the splitting resistance equation adopted by Eurocode 5 for softwoods loaded perpendicular to grain by connections has been studied. It results to be very conservative in predicting the splitting failure load comparing to the experimental data. However, the general analytical model on which this equation is based overpredicts the splitting capacity of the connection when the real fracture parameters of the material are considered ($C_1 = 33{,}14$ N/mm^{1,5} instead of the $C_1 = 14$ N/mm^{1,5} that is set in the EC5 equation). This fact could lead to a dangerous design situation and so require a review for any specific hardwood.

The correlation between the experimental failure loads and theoretically ones predicted by other analytical fracture mechanics models available in literature was also investigated. A model based on quasi-nonlinear fracture mechanics which also included the tension perpendicular to grain strength of the member provided a good agreement with the experimental results for both single and double-dowel connections. It could be considered for further desirable improvements of the design equation.

In all the analytical equations studied, the apparent fracture modulus $\sqrt{GG_c}$ seems to be the mechanical property relevant for the splitting behaviour of the related connections. Therefore, a broad experimental campaign on Mode I and Mode II fracture characterization following the innovative Compliance-Based Beam Method was first carried out, resulting in main fracture energies values of $G_{Ic} = 0{,}77$ (N/mm) and $G_{IIc} = 1{,}66$ (N/mm) respectively for this species. It would be desirable that design standards collect this material parameter for different species, for which rigorous experimental investigations in this respect would be necessary.

2D FEM simulations was also performed for the three single-dowel connection layouts. The numerical model predicted ultimate splitting loads close to the highest experimental ones. It also results in initial stiffness sligthly higher than those despicted by some of the experimental tests. It could be due to possible small dowel deformations that are difficult to measure considering the loading device. The model is therefore planned to be improved in further researchs as it was just a first closeness to it.

The results of this STSM and this report could be considered for further revision and improvement of the design equations and recommendations given in the Eurocode 5 to design connections loaded at an angle to the grain including hardwoods.

7. Future work

From the results obtained in this research, some possible lines of future work are suggested below.

- A broader experimental study of connections loaded perpendicular to grain extended to other hardwoods species would be important in order to better derive a general formula in agreement to all of them. The influence of different connection parameters such as number and diameter of the dowels, connection geometry and position or beam dimensions could thereby being studied. Also other types of fasteners could be studied in detail.
- The 2D numerical model could be improved. Also a 3D model could be developed in order to consider interaction between the fasteners, the failure of the dowels, the local wood plasticity along the fastener´s axis or the border effects affecting the damage initiation along the thickness due to three-dimensional stress fields.
- A parametrical numerical analysis in the framework of Fracture Mechanics by means of a crack propagation approach would be also advisable.
- A comprehensive experimental determination of the fracture energy G_I for each specie or product would be desirable as no values are specified in the standards.

8. Future collaboration with the host institution

In view of the very positive and open collaboration between the involved persons of Technische University of Madrid and the University of Trás-os-Montes e Alto Douro, further collaborations in manifold ways and fields are agreed.

Testing of additional series of connections in Eucalyptus globulus with different layouts are envisaged together. An study of the influencing parameters and background of the analysis in more detail is planned by means of numerical modeling. Considering the solid and advanced experience of host institution in the field of materials fracture characterization, it is aimed to collaborate in extending the experimental campaign to other wood species, specially in hardwoods.

9. Foreseen publications/articles resulting from the STSM

The findings from the experimental and numerical investigations on the splitting capacity of Eucalyptus globulus connections loaded perpendicular to grain, including also further planned work on parametrical modelling, are foreseen to be published in a joint peer-reviewed journal paper.

Also original peer-reviewed journal-paper/s including the research on Mode I and Mode II fracture characterization in Eucalyptus globulus are also envisaged.

In addition, it is amied to disseminate the main findings of this STSM in a conference paper, scheduled to be submitted for oral presentation to the World Conference on Timber Engineering (WCTE 2018, Seoul, Korea).

10. Acknowledgements

I would like to thank the steering committee of the COST Action FP 1402 for giving me the chance of working together with Professors José Morais and Jose Xavier at the University of Trás-os-Montes e Alto Douro. Thanks to them for the fruitful exchange of ideas and their great support during the experimental and numerical program, and also for providing me access to all the facilities of the Department.

The work has been developed within the framework of the research project BIA2015-64491-P *Analysis of the stress relaxation in curved members and new joints solutions for timber Gridshells made out of Eucalyptus globulus*, co-financed by the Ministry of Economy and Competitiveness of Spain Government and ERDF funds.

References

[1] DIN 1052:2008 entwurf, berechnung und bemessung von holzbauwerken- allgemeine bemessungsregeln und bemessungsregeln für den hochbau. berlin, germany.

[2] EN 1912:2012. structural timber - strength classes - assignment of visual grades and species.

[3] EN 1995-1-1:2016. eurocode 5: Design of timber structures.part 1-1: General. common rules and rules for buildings.

[4] EN 408:2011. timber structures- structural timber and glued laminated timber - determination of some physical and mechanical properties.

[5] OS86:2009 engineering design in wood. canadian standards association. mississauga, canada.

[6] prEN 350-2:2014. durability of wood and wood-based products- natural durability of solid wood: Guide to natural durability and treatability of selected wood species of importance in europe.

[7] *CAMBIUM-Aprovechamiento de recursos no maderables en componentes y sistemas de altas prestaciones técnicas (in english: CAMBIUM -Using non-wood resources in technical high-performance components and systems).* IN852A 2013/18. Conecta Peme Program, 2013.

[8] *LIGNUM-Nuevos usos y sistemas para la madera sólida de eucaliptus globulus (in english: LIGNUM-New uses and systems for solid eucalyptus globulus wood).* ITC-20133059. ERDF Innterconecta Program, 2013.

[9] *EUCAGRID-Análisis de la relajación de tensiones en láminas curvadas y de nuevas soluciones de unión para estructuras de madera tipo Gridshell realizadas con Eucalyptus globulus (in english: EUCAGRID-Analysis of the stress relaxation in curved members and new joints solutions for timber Gridshells made out of Eucalyputs globulus).* BIA2015-64491-P. I+D Project. Program for the promotion of scientific research and technique of excellence. Economy and Competitiveness Ministry, 2015.

[10] *XILOGRACILE-Tecnificación de la cadena de valor para el desarrollo de productos de altas solicitaciones técnicas con madera de eucalipto (in english: XILOGRACILE-Value chain technification for the development of technical high-peformance eucalyptus wood products).* ITC-20151124. ERDF Innterconecta Program, 2015.

[11] Leijten A.J.M. and Jorissen A.J.M. Splitting strength of beams loaded by connections perpendicular to grain, model validation. . *In Proceedings of CIB-W18 Conference, paper 34-7-1, The Netherlands.*, 2001.

[12] Leijten A.J.M. and Schoenmakers J.C.M. Timber beams loaded perpendicular to grain by multiple connections. *Engineering Structures*, 80:147–152, 2014.

[13] Franke B. and Quenneville P. Analysis of the failure behaviour of transversely loaded dowe-type connections in wood. *Proceedings of the World Conference on Timber Engineering*, Riva del Garda, Italy, 2010.

[14] Franke B. and Quenneville P. Design approach for the splitting failure of dowel-type connections loaded perpendicular to grain. *In: Proc. of the CIB-W18 Meeting 44*, Vancouver, Canada. Paper No. CIB-W18/44-7-5, 2011.

[15] Franke B. and Quenneville P. Numerical modeling of the failure behavior of dowel connections in wood. *Journal of Engineering Mechanics, ASCE*, 137(3):186–195, 2011.

[16] Franke B. and Quenneville P. Prediction of the load capacity of dowel-type connections loaded perpendicular to grain for solid wood and wood products. *In: Proceedings of the WCTE2012,*, 15-19 July. Auckland, New Zeland., 2012.

[17] Xu B.H., Bouchair A., Taazount M., and Vega E.J. Numerical and experimental analysis of multiple-dowel steel-to-timber joints in tension perpendicular to grain. *Engineering Structures*, 31:2357–2367, 2009.

[18] Santos C.L., de Jesus A.M.P., Morais J.J.L., and Lousada J.L.P.C. Quasi-static mechanical behaviour of a double-shear single dowel wood connection. *Construction and Building Materials*, 23:171–182, 2009.

[19] Santos C.L., Morais J.J.L., and de Jesus A.M.P. Mechanical behaviour of wood t-joints.experimental and numerical investigation. *Frattura ed Integrità Strutturale*, 31:23–37, 2015.

[20] Hindman D.P., Finkenbinder D.E., Loferski J.R., and Line P. Strength of sawn lumber and wood composite connections loaded perpendicular to grain: Fracture mechanics equations. *J. Mater. Civ. Eng.*, 22(12):1226–1234, 2010.

[21] Resch E. and Kaliske M. Numerical analysis and design of double-shear dowel-type connections of wood. *Eng Struct*, 41:234–241, 2012.

[22] Serrano E. and Gustafsson P.J. Fracture mechanics in timber engineering - strength analyses of components and joints. *Mater. Struct.*, 40(1):87–96, 2006.

[23] Silva F.G.A., Morais J.J.L., Dourado N., Xavier J., Pereira F.A.M., and M.F.S.F. de Moura. Determination of cohesive laws in wood bonded joints under mode ii loading using the enf test. *International Journal of Adhesion and Adhesives*, 51:54–61, 2014.

[24] Alfano G. and Crisfield M.A. Finite element interface models for the delamination analysis of laminated composites: Mechanical and computational issues. *Int. J. Numer. Methods Eng.*, 50:1701–1736, 2001.

[25] Petersson H. Fracture mechanics of timber beams and end notches. *Proc., CIB-W18 Meeting 38*, 1995.

[26] Larsen H.J. and Gustafsson P.J. Dowel joints loaded perpendicular to grain. *Proc., Int. Council for Research and Innovation in Building and Construction.*, Rotterdam, Netherlands, 2001.

[27] Ehlbeck J., Görlacher R., and Werner H. Determination of perpendicular to grain stresses in joints with dowel-type fasteners - a draft proposal for design rules. *In: Proc. of the CIB-W18 Meeting 22*, Berlin, Germany. Paper No. CIB-W18/22-7-2, 1989.

[28] Xavier J., Morais J., Dourado N., and de Moura M.F.S.F. Measurement of mode i and mode ii fracture properties of wood-bonded joints. *Journal of Adhesion Science and Technology*, 25:2881–2895, 2011.

[29] Xavier J., Oliveira M., Monteiro P., Morais J.J.L., and de Moura M.F.S.F. Direct evaluation of cohesive law in mode i of pinus pinaster by digital image correlation. *Experimental Mechanics*, 54:829–840, 2014.

[30] Schoenmakers J.C.M. *Fracture and failure mechanisms in timber loaded perpendicular to grain by mechanical connections.* PhD thesis, Univ. of Technology, Eindhoven, Netherlands, 2010.

[31] Williams J.G. The fracture mechanics of delamination tests. *J. Strain Anal*, 24:207–214, 1989.

[32] Jensen J.L. Quasi-non-linear fracture mechanics analysis of splitting failure in moment-resisting dowel joints. *J. Wood. Sci.*, 51(6):583–588, 2005a.

[33] Jensen J.L. Quasi-non-linear fracture mechanics analysis of the splitting failure of single dowel joints loaded perpendicular to grain. *J. Wood Sci.*, 51(6):559–565, 2005c.

[34] Jensen J.L. Splitting strength of beams loaded perpendicular to grain by dowel joints. *J. Wood. Sci.*, 51(5):480–485, 2005d.

[35] Jensen J.L., Girhammar U.A., Quenneville P., and Källsner B. Splitting of beams loaded perpendicular to grain by connections-simple fracture mechanics models. *In: Proceedings of the WCTE2012*, 15-19 July, Auckland, New Zeland., 2012.

[36] Lersen J.L., Quenneville P., Girhammar U.A., and Källsner B. Brittle failures in timber beams loaded perpendicular to grain by connections. *J. Mater. Civ. Eng.*, 27(11):04015026, 2015.

[37] Johansen K.W. Theory of timber connections. *Int Assn Bridge Struct Eng Pub. 9, Zurich, Switzerland*, pages 249–311, 1949.

[38] Ballerini M. A new prediction formula for the splitting strength of beams loaded by dowel-type connections. *In: Proc. of the CIB-W18 Meeting 37*, Edingburgh, Scotland, Paper No. CIB-W18/37-7-5, 2004.

[39] Ballerini M. and Giovanella A. Beams transversally loaded by dowel-type joints: influence on splitting strength of beam thickness and dowel size. *Proceedings of CIB-W18 Conference*, paper 36-7-7, Estes Park, Colorado, USA, 2003.

[40] Ballerini M. and Bezzi R. Numerical lefm analyses for the evaluation of failure loads of beams loaded perpendicular-to-grain by single-dowel connections. *Proceedings of CIB-W18 Conference*, paper 34-7-6, Venice, Italy, 2001.

[41] Kasim M. and Quenneville J.H.P. Effect of row spacing on the capacity of bolted timber connections loaded perpendicular-to-grain. *Proceedings of CIB-W18 Conference*, paper 35-7-6, Kyoto, Japan, 2002.

[42] Snow M., Asiz A., and Smith I. Failure behaviour of single dowel connections in engineered wood products. *5th Structural Specialty Conf. of the Canadian Society for Civil Engineering*, 2004.

[43] Yasumura M. Criteria for damage and failure of dowel-type joints subjected to force perpendicularto-grain. *Proceedings of CIB-W18 Conference*, paper 34-7-9, Venice, Italy, 2001.

[44] Patel M.C. and Hindman D.P. Comparison of single- and two-bolted lvl perpendicular-to-grain connections. ii: Fracture models. *J. Mater. Civ. Eng.*, pages 339–346, 2012.

[45] de Moura M.F.S.F., Morais J.J.L., and Dourado N. A new data reduction scheme for mode i wood fracture characterization using the double cantilever beam test. *Eng Fract Mech*, 75(13):3852–3865, 2008.

[46] de Moura M.F.S.F., Silva M.A.L., de Morais A.B., and J.J.L. Morais. Equivalent crack based mode ii fracture characterization of wood. *Engineering Fracture Mechanics*, 73(8):978–993, 2006.

[47] Dourado N.M.M., de Moura M.F.S.F., Morais J.J.L., and Silva M.A.L. Estimate of resistance-curve in wood through the double cantilever beam test. *Holzforschung*, 64:119–126, 2010.

[48] Borth O. and Rautenstrauch K. Estimation of the load-carrying capacity of perpendicular-to-grain bolted timber connections by fracture criterion in the framework of lefm. *Proceedings of the International RILEM Symposium on Joints in Timber Structures*, Stuttgart, Germany, 2001.

[49] Gustafsson P.J. Fracture perpendicular to grain - structural applications. *In: Timber Engineering*, S. Landersson and H.J. Larsen, eds., Wiley, Chichester, U.K., 2003.

[50] Reske R.G., Mohammad M., and Quenneville J.H.P. Influence of joint configuration parameters on strength of perpendicular-to-grain bolted timber connections. *Proceedings of the World Conference on Timber Engineering*, Whistler, B.C., Canada, 2000.

[51] Itany R.Y. and Faherty K.F. Structural wood research, state-of-the-art and research needs. *ASCE,*, New York, 210., 1984.

[52] Franke S. and Marto J. Investigation of eucalyptus globulus wood for the use as an engineered material. *Proceedings of the World Conference on Timber Engineering*, Quebec, Canada., 2014.

[53] van der Put T.A.C.M. Tension perpendicular to the grain at notches and joints. *Proc. of the CIB-W18 Meeting 23*, Lisbon, Portugal, Paper No. CIB-W18/23-10-1, 1990.

[54] van der Put T.A.C.M. and Leijten A.J.M. Evaluation of perpendicular to grain failure of beams caused by concentrated loads of joints. *Porc. Int. Council for Research and Innovation in Building and Construction*, Rotterdam, Netherlands, 2000.

[55] Caldeira T.V.P., Dourado N., de Jesus A.M.P., de Moura M.F.S.F., and Morais J.J.L. Quasi-static behavior of momento-carrying steel-wood doweled joints. *Construction and Building Materials*, 53:439–447, 2014.